# Model Predictive Speed Control of a Permanent Magnet Synchronous Motor for Electric Vehicle (case study on Hyundai ATOS)

Mulugeta Hintsa Kebedew

A Thesis Submitted to

The Department of Electrical Power and Control Engineering

School of Electrical Engineering and Computing

Presented in Partial Fulfillment of the Requirement for the Degree of Master's in Electrical Power and Control Engineering (Control Engineering)

Office of Graduate Studies

Adama Science and Technology University

June, 2023

Adama, Ethiopia

# Model Predictive Speed Control of a Permanent Magnet Synchronous Motor for Electric Vehicle (case study on Hyundai ATOS)


Mulugeta Hintsa Kebedew

Advisor: Professor Seungnam Kim


A Thesis Submitted to
The Department of Electrical Power and Control Engineering
School of Electrical Engineering and Computing

Presented in Partial Fulfillment of the Requirement for the Degree of Master's in Electrical Power and Control Engineering (Control Engineering)


Office of Graduate Studies
Adama Science and Technology University


June, 2023

Adama, Ethiopia

# DECLARATION

I declare that this Master Thesis entitled "Model Predictive Speed Control of a Permanent Magnet Synchronous Motor for Electric Vehicle (case study on Hyundai ATOS)" is my original work. That is, it has not been submitted for the award of any academic degree, diploma or certificate in any other university. All sources of materials that are used for this thesis have been duly acknowledged through citation.

| | | |
|---|---|---|
| Mulugeta Hintsa Kebedew | ____________________ | _________________ |
| Name of Student | Signature | Date |

# RECOMMENDATION OF ADVISOR

I, the major advisor of this thesis, hereby certify that I have read the revised version of the thesis entitled "Model Predictive Speed Control of a Permanent Magnet Synchronous Motor for Electric Vehicle (case study on Hyundai ATOS)" prepared under my guidance by Mulugeta Hintsa Kebedew submitted in partial fulfillment of the requirements for the degree of Mater's of Science in Control Engineering. Therefore, I recommend the submission of revised version of the thesis to the department following the applicable procedures.

| | | |
|---|---|---|
| Professor Seungnam Kim | ____________________ | _________________ |
| Major Advisor | Signature | Date |

# APPROVAL PAGE

I, the advisors of the thesis entitled "Model Predictive Speed Control of a Permanent Magnet Synchronous Motor for Electric Vehicle (case study on Hyundai ATOS)" and developed by Mulugeta Hintsa Kebedew, hereby certify that the recommendation and suggestions made by the board of examiners are appropriately incorporated into the final version of the thesis.

| | | |
|---|---|---|
| Professor Seungnam Kim | ____________________ | _________________ |
| Major Advisor | Signature | Date |

We, the undersigned, members of the Board of Examiners of the thesis by Mulugeta Hintsa Kebedew have read and evaluated the thesis entitled "Model Predictive Speed Control of a Permanent Magnet Synchronous Motor for Electric Vehicle (case study on Hyundai ATOS)" and examined the candidate during open defense. This is, therefore, to certify that the thesis is accepted for partial fulfillment of the requirement of the degree of Master of Science in Control Engineering.

| | | |
|---|---|---|
| _______________________ | ____________________ | _________________ |
| Chairperson | Signature | Date |
| _______________________ | ____________________ | _________________ |
| Internal Examiner | Signature | Date |
| _______________________ | ____________________ | _________________ |
| External Examiner | Signature | Date |

Final approval and acceptance of the thesis is contingent upon submission of its final copy to the Office of Postgraduate Studies (OPGS) through the Department Graduate Council (DGC) and School Graduate Committee (SGC).

| | | |
|---|---|---|
| _______________________ | ____________________ | _________________ |
| Department Head | Signature | Date |
| _______________________ | ____________________ | _________________ |
| School Dean | Signature | Date |
| _______________________ | ____________________ | _________________ |
| Office of Postgraduate Studies, Dean | Signature | Date |

# ACKNOWLEDGEMENT

First and foremost, I want to express my gratitude to the Almighty GOD for providing me the strength. And, I am deeply grateful to my advisor Professor Seungnam Kim for their invaluable guidance and mentorship throughout my thesis work. Their expertise, insight feedback and constant encouragement have been instrumental in shaping this thesis. I am also thankful to my instructors Dr. Endalew A. and Dr. Tefera T. for their constructive comments and valuable suggestions that helped me on the research methodology and enhance the quality of this work. I extend my appreciation to the department of EPCE for providing the necessary resource, computer lab, and opportunities that supported my thesis endeavors.

My heartfelt thanks go to my family and friends for their unwavering support and understanding throughout this challenging journey. Their belief in me and their constant encouragement provided the motivation I needed to persevere.

# Table of Contents


DECLARATION ........ i

RECOMMENDATION OF ADVISOR ........ ii

APPROVAL PAGE ........ iii

ACKNOWLEDGEMENT ........ iv

LIST OF TABLES ........ viii

LIST OF FIGURES ........ ix

LIST OF ABBREVIATIONS ........ xi

ABSTRACT ........ xii

CHAPTER ONE ........ 1

1. INTRODUCTION ........ 1

1.1. Background of the Study ........ 1

1.2. Statement of the problem ........ 2

1.3. Objectives ........ 3

1.3.1. General Objective ........ 3

1.3.2. Specific Objective ........ 3

1.4. Scope of the study ........ 3

1.5. Significance of the study ........ 4

1.6. Limitation of the Study ........ 4

1.7. Thesis organization ........ 4

CHAPTER TWO ........ 6

2. LITERATURE REVIEW ........ 6

2.1. Background of Electric Vehicles ........ 6

2.1.1. Electric Vehicles Drivetrain ........ 7

2.2. Trends of Electric Motors for EVs ........ 8

2.2.1. DC Motors ........ 8

2.2.2. Induction Motors ........ 9

2.2.3. BLDC Motors ........ 10

2.2.4. Reluctance Motors....10

2.2.5. Permanent Magnet Synchronous Motor (PMSM)....11

2.3. Related Works ....12

2.4. Overview of GA and PI Controller....16

2.5. Overview of LQR Controller....17

2.6. Overview of MPC....17

CHAPTER THREE....19

3. METHODOLOGY....19

3.1. Overview....19

3.2. Materials ....19

3.3. Methods ....19

3.4. The Block Diagram of proposed PMSM drive for EV ....20

3.5. Electric Vehicle Dynamics ....20

3.5.1. Motive Force, Power and Torque of Hyundai ATOS Vehicle....21

3.5.1.1. Tire Rolling Resistance Force....22

3.5.1.2. Aerodynamic drag Force ....22

3.5.1.3. Gradient (Climbing) Resistance Force ....23

3.5.1.4. Torque required on the drive wheel....25

3.6. Mathematical Model of PMSM drive....27

3.6.1. Reference Frame Transformation....27

3.6.2. Three-phase Equivalent Circuit of PMSM....29

3.6.3. Model and dq0 Equivalent Circuit of PMSM ....30

3.6.4. State Space Model of a PMSM ....32

3.7. Space Vector Pulse Width Modulation (SVPWM) ....32

CHAPTER FOUR....35

4. CONTROLLER DESIGN....35

4.1. Current Inner Loop PI controller ....35

4.2. Speed Outer Loop PI Controller ....35

4.3. Speed Outer Loop LQR Controller....36
4.4. Speed Outer Loop MPC Controller....37
4.4.1. Constraint on Control Input....40
4.4.2. Constraint on the Optimal Solution....41
4.4.3. Constraint on the Output Variable....42
CHAPTER FIVE....46
5. SIMULATION RESULT AND DISCUSSION....46
5.1. Simulation Result of a PMSM without Vehicle Load....46
5.2. Set Point Change of a PMSM with Vehicle Load....50
5.3. Speed Changes on a PMSM with Vehicle Load....52
5.4. Disturbance Rejection Rerformance of the Controllers....53
5.5. Electromagnetic Torque of a PMSM....54
5.6. Simulation Result of SVPWM and Inverter....56
6. CONCULSION AND RECOMMENDATION....57
6.1. Conclusion....57
6.2. Recommendation....57
REFERENCES....60
APPENDICES....65

# LIST OF TABLES

Table 2-1: Performance comparison of motor drives ........ 11
Table 2-2: Summary of literature review ........ 15
Table 3-1: Hyundai ATOS car specification[L7] ........ 21
Table 3-2: Values of rolling resistance coefficient (S Chauhan et al.,2015) ........ 22
Table 3-3: PMSM parameter specification ........ 26
Table 3-4: Eight possible switching states ........ 33

# LIST OF FIGURES

Figure 2-1: Global Electric vehicle Sales (Oubelaid et al., 2022) ........ 6
Figure 2-2. Motor options for the EV drive application ........ 8
Figure 2-3: DC motor [L3] ........ 9
Figure 2-4: Induction Motor [L4] ........ 9
Figure 2-5: BLDC motor ........ 10
Figure 2-6: Switch Reluctance Motor [L5] ........ 10
Figure 2-7: (a) Surface Mounted PMSM (b) Interior PMSM ........ 11
Figure 2-8: Schematic diagram LQR controller [L6] ........ 17
Figure 2-9: Schematic diagram of MPC ........ 18
Figure 3-1: Block diagram of the research methodology ........ 19
Figure 3-2: Block diagram of the proposed control system ........ 20
Figure 3-3: Free body diagram of Hyundai ATOS vehicle ........ 21
Figure 3-4: Motive forces verses approaching angle ........ 25
Figure 3-5: Desire total power verses speed of car in kph ........ 25
Figure 3-6: Three and two-phase stator winding ........ 27
Figure 3-7: Clarke-Park transformation ........ 28
Figure 3-8: Stator circuit of a PMSM ........ 29
Figure 3-9: PMSM d-q axis equivalent circuit ........ 30
Figure 3-10: Three-phase inverter ........ 32
Figure 3-11: Space vector hexagon with basic voltage vector ........ 33
Figure 3-12: Output voltage as adjacent vector in sector 1 ........ 34
Figure 3-13: Switching time for sector 1 ........ 34
Figure 4-1: PI current controller ........ 35
Figure 4-2: PI speed controller ........ 35
Figure 5-1: Rotor speed and desired speed using MPC, LQR and GA-PI without vehicle load ........ 47
Figure 5-2: Outer loop Control signal of MPC, LQR and GA-PI ........ 48
Figure 5-3: Error between desired and actual speed of a PMSM without vehicle load ........ 48
Figure 5-4: d-q Current response without vehicle load ........ 49
Figure 5-5: Voltage Vd-q response ........ 49
Figure 5-6: Rotor speed and desired speed using MPC, LQR and GA-PI with vehicle load ........ 50

Figure 5-7: Error between desired and actual speed of a PMSM with vehicle load ........... 51
Figure 5-8: d-q Current response with vehicle load ........................................................... 51
Figure 5-9: Vdq voltage with vehicle load ........................................................................ 52
Figure 5-10: Result of speed variation of a PMSM for case-1 ........................................... 52
Figure 5-11: Result of speed variation of a PMSM for case-2 ........................................... 53
Figure 5-12: Rotor speed with disturbance uphill case ...................................................... 53
Figure 5-13: Rotor speed with disturbance load variation case.......................................... 54
Figure 5-14: Electromagnetic torque with vehicle load ...................................................... 54
Figure 5-15: Electromagnetic torque uphill disturbance case ............................................. 55
Figure 5-16: Electromagnetic torque under speed variation ............................................... 55
Figure 5-17: PWM duty cycle ............................................................................................ 56
Figure 5-18: Three phase voltage source from inverter ...................................................... 56

# LIST OF ABBREVIATIONS

| | |
|---|---|
| AC | Alternative current |
| BLDC | Brushless direct current |
| DC | Direct current |
| EV | Electric vehicle |
| FOC | Field oriented control |
| GA | Genetic algorithm |
| GPC | General predictive control |
| ICE | Internal combustion engine |
| IM | Induction motor |
| IPMSM | Interior permanent magnet synchronous motor |
| LQR | Linear quadratic regulator |
| MPC | Model predictive control |
| NMPC | Nonlinear model predictive control |
| PI | Proportional integral |
| PID | Proportional integral derivative |
| PMSM | Permanent magnet synchronous motor |
| PSO | Particle swarm optimization |
| PWM | Pulse width modulation |
| SMC | Sliding mode control |
| SPMSM | Surface mounted permanent magnet synchronous motor |
| SRM | Switch reluctance motor |
| SVPWM | Space vector pulse width modulation |

# ABSTRACT

*Currently, electric vehicles (EVs) are a popular and rapidly growing solution to reduce emissions from our transportation sector. With this inspiration, this thesis presented an approach to develop model predictive speed control of a permanent magnet synchronous motor (PMSM) for the application of EV. According to the specification of the Hyundai ATOS vehicle which analyzed the different forces imposed to the vehicle, the power required to overcome these forces and the torque required to propel the vehicle. Then, due to the power and torque requirements the motor is selected. The control method model predictive control (MPC) is designed for the outer loop speed control and proportional integral (PI) for the inner loop current control based on the developed dynamic model of the PMSM drive system by considering input output constraints. The outer loop is responsible for regulating the speed of the motor while the inner loop focuses on maintaining the current or torque. To ensure the effectiveness of the proposed method, MPC is compared with linear quadratic regulator (LQR) and genetic algorithm based proportional integral (GA-PI) control approaches. And GA technique is used to tune the parameters of the PI gain and the weighting matrix of the cost function. As a simulation result the proposed MPC obtained better performance and effective than LQR and GA-PI. And also, MPC has no overshoot, better steady state performance and anti-load disturbance capability which shows the effectiveness of the proposed strategy.*



***Keywords****: MPC, PMSM, Hyundai ATOS vehicle, LQR and GA-PI*

# CHAPTER ONE

# 1. INTRODUCTION

## 1.1. Background of the Study

The history of electric vehicles (EVs) years back to the 1830s when Scottish inventor Robert Anderson built the first crude electric carriage [L1]. However, it was not until the late 1800s and early 1900s that EVs gained popularity, particularly in the United States and Europe. Over the last 160 years, improvements in technology resulted in various versions of EVs coming into the market. EVs were mostly popular for their quiet and smooth operation, and were used for everything from personal transportation to commercial delivery vehicles. However, the popularity of EVs began to decline in the 1920s and 1930s [L2], as improvements in internal combustion engine technology led to the mass production of affordable gasoline-powered cars. Additionally, advancements in road infrastructure made gasoline refueling more convenient, while the limited range and long recharging times of early EVs made them less practical for long-distance travel. Despite this decline in popularity, EVs continued to be used in certain niche applications, such as golf carts, forklifts, and other small vehicles that operate in limited areas. In the 1960s and 1970s, the world concerned about air pollution and oil dependence, so they concentrate to refine their interest in EVs, leading to the development of several experimental models with improved battery technology. In recent years, EVs have seen a resurgence in popularity due to concerns about climate change and efforts to decrease greenhouse gas emissions. (Varga et al., 2019) As technology continues to improve dramatically over time, eventually allowing for increased range capabilities as well as faster charging times, it will be interesting to watch how far EV technology advances over the next decade and beyond that. In addition to reduced environmental impacts, several other benefits make switching to an EV appealing, such as increased vehicle efficiency, longer drive range on a single charge, lower maintenance costs, potential utility bill savings from charging the vehicle at off-peak rates, and quiet operation. Given all the advantages of EVs over internal combustion engine vehicles, it is unsurprising why there is an increasing interest in these eco-friendly options.

Electric motors are a fundamental component of EVs as they provide the necessary power for propulsion (Murali et al., 2021). These motors operate according to the electromagnetic principle, which transforms electrical energy into mechanical energy. There are several types of electric motors used in EVs. The most common types are, induction motor, permanent magnet synchronous motor (PMSM), brushless direct current motor and switch reluctance motor, the selection of the electric motors depends on the different factor(Cao et al., 2019). In this study PMSM is selected due to their high-power density, high efficiency, compact size, and high torque inertia ratio(X. Huang et al., 2020). Additionally, PMSMs have a higher power factor, which means that less reactive power is needed to run them. This decreases the amount of power that needs to be produced and transmitted, resulting in lower energy costs(Yang et al., 2020). Another advantage of PMSMs is their speed control capabilities. They can achieve precise speed control and torque regulation, which makes them appropriate for applications where precise control is required.

As focusing on the EV, it is critical to regulate the motor to get appropriate speed and torque profiles for the EV. An essential reason is that the torque and speed fluctuating throughout the ride. Therefore, the PMSM control method must have an excellent dynamic response to handle changing input. There are several control approaches present to control PMSM. The most known control strategy is field oriented control (FOC), which has a slow dynamic response for the application of EVs. Sliding mode control (SMC), linear quadratic regulator (LQR), intelligent control and other strategy applied to control the PMSM as gathering in different literatures. In recent years, many researches concentrate on the application of model predictive control approach in PMSM control. MPC is an advanced control strategy that uses a mathematical model of the system to predict the future behavior and optimize the control action (Gao et al., 2021). The basic future of MPC is to minimize the cost function that captures the desired behavior of the system over finite prediction horizon while satisfying a set of constraints on the system state and control inputs.

This thesis focuses on the speed control, and consequently the current control also considered as the motor system configuration. MPC utilized on the outer loop speed control and GA based PI applied in the inner current control of the PMSM model. And also compared GA-PI and LQR method with the proposed MPC strategy for speed control of PMSM while the inner loop current controlled by PI controller.

### 1.2. Statement of the problem

The conventional vehicles are used internal combustion engine (ICE) for propulsion purpose which are powered by fossil fuel and have several disadvantages compared to EVs. For example, environmental pollution, dependency on non-renewable fossil fuel and noise pollution. From this initiation, this thesis preferred the most common and affordable non-electric vehicle Hyundai ATOS car as a case to provide a proper motor.

EVs are used an electric motor as a propulsion. From different types of electric motors, the widely used PMSM is selected for this thesis due to their high efficiency, high density, small size and less torque ripple. In particular, the speed of a PMSM in EV application presents a significant challenge that requires an effective solution. Conventional control approaches, like PI control or FOC, have a limitation in terms of achieving accurate speed regulation and accommodating various operational constraints. PI control and FOC have limited performance at high speed operation, PMSM operating at high speeds may experience saturation effects which can impact the accuracy and effectiveness controllers. These limitations can affect the overall performance and responsibility of the PMSM for an EV application. To address the challenges, there is a need an advanced and optimal control strategy like model predictive control (MPC) to provide precise speed control and handling constraints associated with motor. The specific problem to be addressed is to develop an effective MPC method for PMSM in Hyundai ATOS vehicle application that can overcome the limitation of conventional control techniques and provide better performance in terms of accuracy and robustness. Additionally, performing a comparison with conventional GA-PI and LQR optimal control is another contribution of the thesis.

## 1.3. Objectives

### 1.3.1. General Objective

The general objective of this thesis is to study and develop model predictive speed control of a PMSM for electric vehicle propulsion in Hyundai ATOS case.

### 1.3.2. Specific Objective

The following specific objective are listed to achieve the main objective of this thesis work.

- Analyzing model of the vehicle in the case of Hyundai ATOS car
- Analyzing dynamic model of PMSM
- Designing model predictive control for speed control of a PMSM
- Performance comparison of LQR and GA-PI controller with the proposed MPC
- Verifying control performance using simulation software MATLAB package

## 1.4. Scope of the study

As mentioned on the objective, the first scope is analyzed the imposed forces and the required power from the Hyundai ATOS car model. According to the power requirement the proper PMSM was selected. After the selection of the motor, provided the mathematical model of PMSM and designed MPC cascading with GA based PI controller using the model.

Moreover, the proposed controller was considered constraints on the control input and output variable to improve the speed performance of the motor. And finally, the performance of the proposed MPC is compared and discussed with an optimal control LQR and conventional control method GA based PI through simulation software MATLAB/Simulink.

### 1.5. Significance of the study

Nowadays, people are alarmed about the negative impact of vehicles on the environment. At the same time there is a huge concern on the frequent shortage of fuel availability. Thus, EVs are miraculous solution to solve this problem, as it utilizes electric motors for propulsion purpose and can be powered by DC or AC source.

Selecting the appropriate motor by analyzing the traction system of the car using the specification is one importance of the study. This thesis also focuses on the modification of the performance of speed of the PMSM. The motor's speed and current are controlled by MPC and PI controller respectively. Hence the significance of this study to upgrade the current Hyundai ATOS in to Electric vehicle is enormous.

Furthermore, this thesis might be useful to support ASTU Center of Transportation and Vehicle Engineering (CTVE) and E-Bajaj center of excellences, because they are engaged in designing and developing electric vehicles. This will in turn contribute to the rising effort of the country automotive technology. Its significance is even more prominent in Ethiopia as the demand for vehicle is increasing radically.

### 1.6. Limitation of the Study

As EVs have several components, this thesis is limited on the control of speed and current of PMSM. Due to time, budget and the difficulty to get components for implementation, the system model is interacted and tested via simulation method through MATLAB/Simulink package.

### 1.7. Thesis organization

This thesis work is organized in six chapters.

**Chapter 1:** Background of the study, problem statement, objective, scope and significance of the study are clearly described.

**Chapter 2:** The history of EVs, trends of common electric motors for EVs, overview of the proposed controller and related recent research papers are well reviewed and explained in this chapter.

**Chapter 3:** Analyzation of the dynamic model of the Hyundai ATOS car through free body diagram and mathematical model of PMSM are clearly derived in this chapter.

**Chapter 4:** Controller design is performed in this chapter.

**Chapter 5:** Simulation result is analyzed and discussed in this chapter.

**Chapter 6:** In this section, conclusion and recommendation are illustrated.

# CHAPTER TWO

# 2. LITERATURE REVIEW

In this chapter, the background of electric vehicles, overview of common electric motors that applicable for electric vehicles (EVs), overview of controllers, and related recent research works are reviewed and discussed.

## 2.1. Background of Electric Vehicles

EVs are automobiles that are powered by electric motors and rechargeable battery packs instead of traditional internal combustion engine (ICE) (Murali et al., n.d.2021). EVs provide several advantages over ICE vehicles, such as lower operating costs, reduced greenhouse gas emissions, and improved energy efficiency (Muthukumar et al., 2021). For the past 20 years, the popularity of EVs has increased for a variety of factors, including awareness of climate change, technological breakthroughs, and industrial growth. There are three types of EVs. Those are; full electric vehicles (powered by electric motors and batteries), hybrid EVs (have both gasoline and electric motors, the electric motor helps to power the car at low speed and when the vehicle is stopped) and the last one is plug-in hybrid EVs (similar with hybrid EVs but can also be plugged into electric power sources to charge). EVs are becoming more affordable and accessible to the average person. Tesla, Nissan, and Volkswagen are just some of the big electric car manufacturers making electric cars for a while now. With decreasing prices of electric batteries, growing accessibility to changing infrastructure, technological advancements, and increasing popularity among consumers, it is likely that electric vehicles will become increasingly common and dominant transportation in our world in the coming years. The remarkable growth rate is the relative base volume of 2020, hybrid EV and full EV sales in 2019, 2020 and in 2021 they returned back to trend, as it is show in the Figure 2-1.

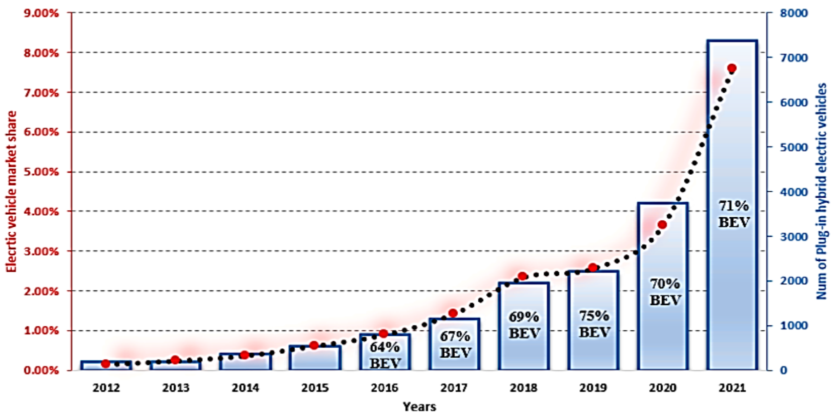


*Figure 2-1: Global Electric vehicle Sales* (Oubelaid et al., 2022)

### 2.1.1. Electric Vehicles Drivetrain

The drive train of the EVs is the system that transmits power from the electric motor to the wheels, enabling the vehicle to move. The drive train of an EV typically includes several components such as the battery, electric motor, transmission, and inverter(Kumar et al., 2022).

The battery is the primary source of energy for electric vehicles. It stores electricity from an external power source and supplies it to the electric motor. The battery size and capacity will determine how far an electric vehicle can travel on a single charge. The types of battery used play a significant role in determining the range, performance, and overall cost of the vehicle. There are different types of batteries available for EVs(Deng et al., 2020). The most common types of battery used in EVs are Lithium-ion (Li-ion). Nickel-Metal Hydride (NiMH), and Lead-Acid. Li-ion batteries are commonly the most popular choice for EVs due to their high energy density, low self-discharge rate, and long cycle life. Li-ion batteries are more efficient than other types of batteries, which means that they can convert a higher percentage of the stored energy into motion. However, battery technology is rapidly advancing and new types of batteries such as the solid-state battery is currently being developed which could offer greater performance and efficiency in the future.

The electric motor is the heart of the EVs drivetrain. It converts electrical energy from the battery into mechanical energy, which drives the wheels of the vehicle. Several types of electric motors are used for electric vehicle propulsion(Cao et al., n.d.2019). The different types of electric motors with their classification are well explained in the following sub topic.

The transmission in an EV is responsible for regulating the torque and speed of the electric motor. Unlike traditional vehicles (ICE) that require complex mechanical transmissions but EVs typically have a single-speed transmission, which is simpler and more efficient.

The inverter is a critical component of the electric drivetrain as it converts the DC power stored in the battery into AC power used for the electric motor. The inverter also controls the amount of power supplied to the motor allowing the driver to control the vehicle's speed and acceleration.

In general, the electric drivetrain is a complex system that requires careful engineering and design to optimize the performance and efficiency.

### 2.2. Trends of Electric Motors for EVs

Electric motors are a fundamental and essential part of EVs, its purpose is to propulsion the vehicle. They need to operate in a harsh environment with a humidity of up to 85% and an environment temperature range of -40° to 135°. (Cao et al., 2019) This is a particular application for EVs where electric motors are close to the ICE. High driving duty cycle, wide constant-power range, and high torque density are further characteristics. These requirements for EV drives should be matched by the output characteristics of an electric motor. Typically, EVs needs the motor to generate a peak torque (during starting, acceleration, or hill climbing) which is 5-10 times the torque for cruising (Magazine & 2017,), (Guan et al.,2014). As several researches studied DC motors, induction motors, PM motors, and reluctance motors have been widely used for EVs propulsion. The general classification of electric motors is summarized in the following diagram.

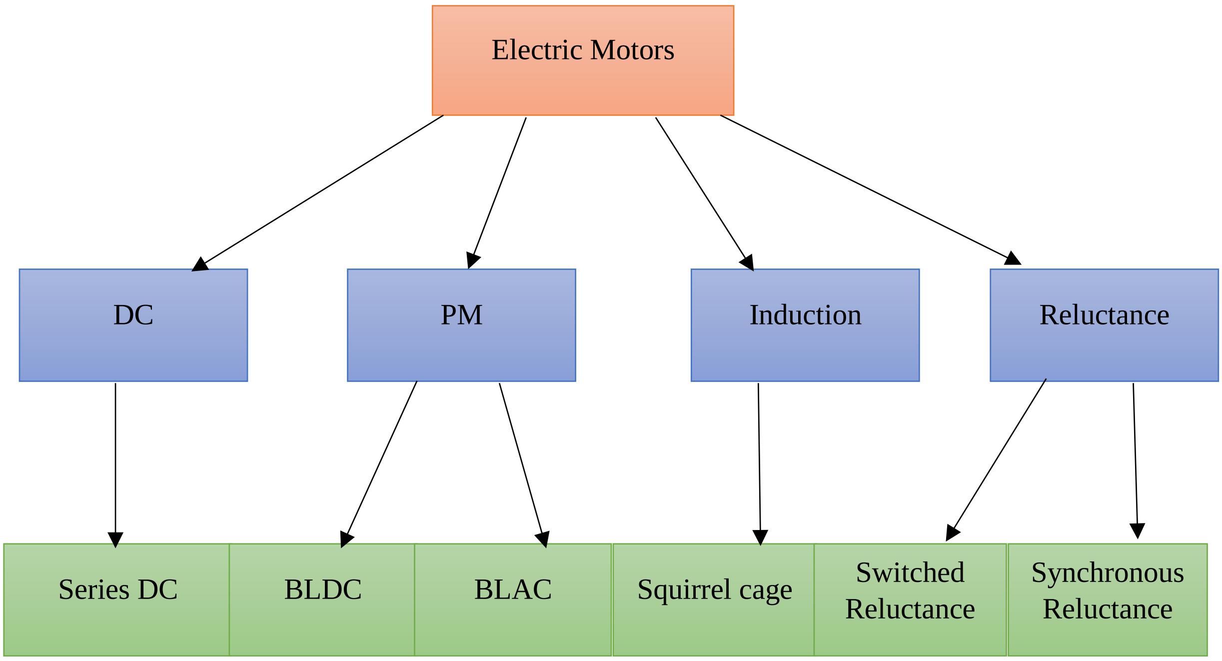


*Figure 2-2. Motor options for the EV drive application*

#### 2.2.1. DC Motors

Early electric vehicles nearly exclusively employed DC motor drives. Simply because the battery in vehicles provided the DC supply. This covered the development and gradual refinement of DC machine technologies. DC motors have good torque-speed characteristics and are easy to control the speed. However, its drives have a complex construction, due to the mechanical commutator needing high maintenance, and low reliability. There are several types of DC motors, including brushed and brushless motors. Brushed motors have a simpler construction and they are less expensive than brushless motors. But they need a regular maintenance and have lower durability. Brushless motors are more efficient, have longer lifespans, and require less maintenance. But they are more complex and more expensive. Despite this, some modern EVs still used DC motors.

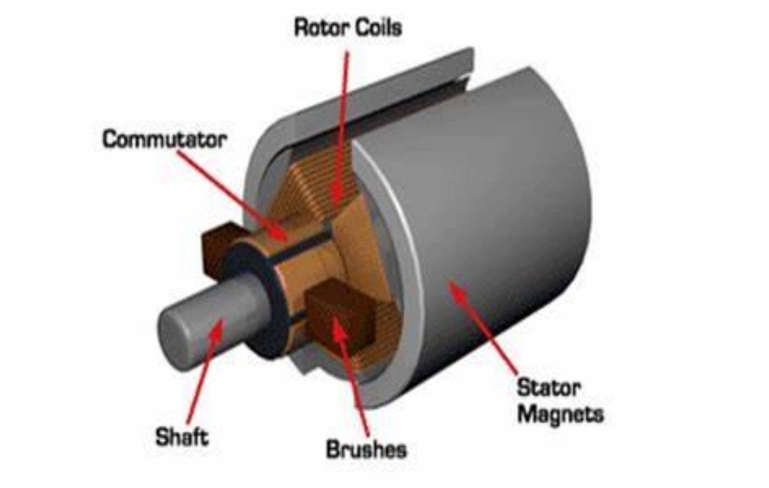


*Figure 2-3: DC motor [L3]*

### 2.2.2. Induction Motors

Induction motors (IMs) are constructed with three-phase AC windings formulated on the stationary part and short-circuit windings on the rotor as shown in the Figure 2-4. IMs are preferred with comparing brushed electric machines. Because brushed electric machines have high maintenance. It is commonly admitted that squirrel-cage IMs are recognized for their simplicity, reliability, cheapness, and robustness because of that they are often employed in industrial drives (Aja Zarma et al., 2019). IM drives are preferred in EV propulsion applications due to their low cost, high reliability, mature manufacturing, and power converter technologies, according to a thorough review of EV motor drives and a survey of experts' viewpoints. However, their drawbacks are low efficiency, low power factor, and low inverter usage, which prevents them from being used in EVs with big motor drives or high-speed operations.

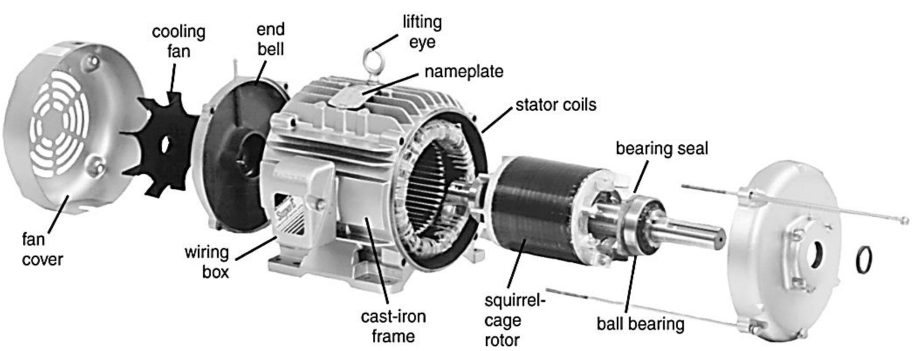


*Figure 2-4: Induction Motor [L4]*

### 2.2.3. BLDC Motors

Electronically commutated BLDC motors are an improvement over brushed DC motors. It is a synchronous motor that a used DC source. A typical BLDC has permanent magnets which rotate around a fixed armature. A brushless motor has several advantages over brushed motors, including high speed, high efficiency, low maintenance, good speed and torque control. It also has a compact size with a high-power density and high efficiency as compared to other motors(Rauth & Samanta, 2020). But its disadvantage is the limited power application as its torque may decrease in increased speed when dealing with higher load. It also generates vibration and noise due to the presence of torque ripple.

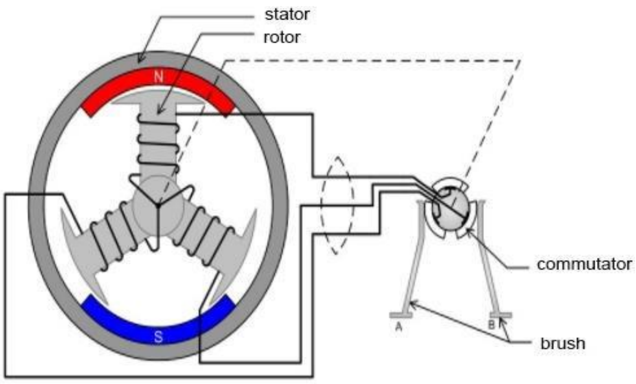


*Figure 2-5: BLDC motor*

Source: (Hasan et al., 2020)

### 2.2.4. Reluctance Motors

Reluctance motor is one of the types of electric motors which have a distinctive rotor structure that is coordinated from laminated silicon steel. The rotor is salient and works using reluctance torque. Synchronous reluctance motors are those that have a round structure and are powered by a multiphase AC source. They have a high-speed range that can run up to seven times as fast as their base speed(Cao et al., 2019). It is especially beneficial for electric vehicles.

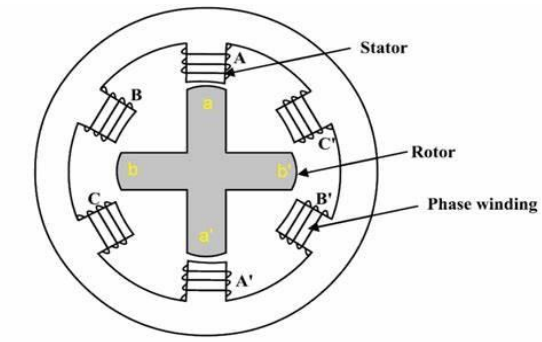


*Figure 2-6: Switch Reluctance Motor [L5]*

### 2.2.5. Permanent Magnet Synchronous Motor (PMSM)

PMSM has a mounted permanent magnet on the rotor and AC three-phase winding on the stator. The construction of PMSM is similar to the synchronous motor rather there is no field winding on the PMSM rotor part. The PMSM is supplied by sinusoidal shape AC current. The figure 7 (a) shows the surface-mounted PMSM, this design offers the largest air gap flux density as it directly faces the air gap. The inductance variation between the quadrature and direct axis is very small in this machine. Figure 7 (b) shows the interior PMSM the magnet placed in the middle of the rotor lamination. (Krishnan, 1991)The IPMSM is mechanically robust and suited for high-speed application. The construction design is more complex than SPMSM. Overall, PMSMs are preferable for EVs propulsion because of their high-power density, high efficiency, high torque to inertia, low weight, and small size. PMSM drives are widely used in recent EVs like Nissan, Hyundai, and Honda.

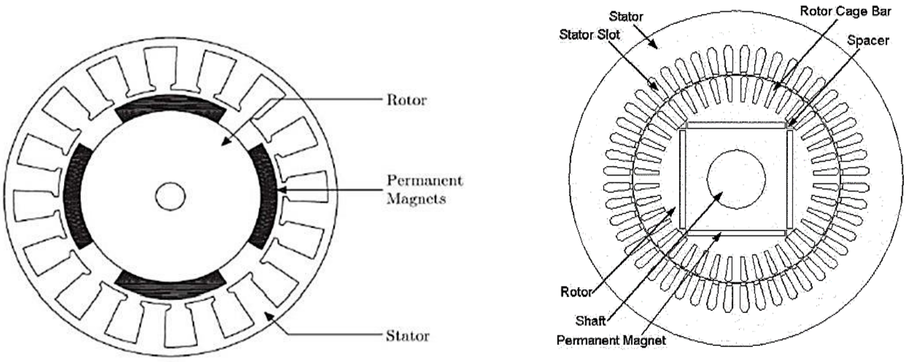


*Figure 2-7: (a) Surface Mounted PMSM (b) Interior PMSM*

Source: (Zhu et al., 2012)

In investigated the performance comparison of different electric motor drives and illustrated in the following table (Cao et al.,2019).

*Table 2-1: Performance comparison of motor drives*

| Performance | DC motor | SRM | IM | PM |
|---|---|---|---|---|
| Power density | Low | Medium | Low | High |
| Torque ripple | Low | High | Low | Medium |
| Acoustic noise | Medium | High | Low | Low |
| Overload capacity | High | Low | High | Medium |

| | | | | |
|---|---|---|---|---|
| Max speed | Medium | Very High | High | Low |
| Speed range | Medium | High | Medium | Low |
| Controllability | High | Low | High | Medium |
| Reliability | Low | High | High | Medium |
| Efficiency | Low | Medium | Medium | High |
| Size | Medium | Large | Medium | Small |
| Cost | Medium | Medium | Low | High |

According to the reviewed of the different electric motor drive PMSM is selected for this thesis work to the electric vehicle propulsion. The motor is selected by it has high efficiency, high power density, and small size.

### 2.3.Related Works

A summary of literatures published regarding the speed control of PMSM with and without electric vehicle is reviewed as follows.

In (Sudjoko et al., 2020) presented the conventional proportional integral derivative (PID) controller to control the speed of PMSM. This paper provides an overview of the PMSM model with characteristics and has a detailed explanation of the proposed control strategy which is PID, a bridge circuit, and a power inverter. The authors present the simulation results to demonstrate the effectiveness of the proposed method. So, the result suggests that the system is effective in controlling the speed of the motor.

In (G. Huang et al., 2022) proposed a control approach for the PMSM drive system using general predictive control (GPC) and equivalent input disturbance (EID). The authors discussed the control strategy in detail to achieve better disturbance rejection. The simulation results were implemented to show the proposed mothed in terms of disturbance and tracking performance. But, one limitation of the paper is that focuses only on the nominal state for the control of the speed of the motor because of the PMSM nonlinearity behavior. For this case, EID method is introduced to solve the problem that happens by load torque and other disturbances. This may not applicable for such high load and operating in a different speed like electric vehicles.

In (Ren et al., n.d.) fuzzy-PID controller is established a self-tuning to meet the required control parameters. Using vector control method shows an improved response performance that obtain minimized steady state error and reduced overshoot. The proposed system is simulated in MATLAB/Simulink and analyzed the results. And they compare with a conventional PID control system and the proposed system has better control performance.

The paper (Gao et al., 2021) proposes an improved MPC for the PMSM drive system based on the state transition constraint method. The probability constraint error term was considered by computing the transition probability of the switch transfer historical data in the MPC cost function, which exports the control vector of a PMSM system. Using the Markov chain method to find out the probability of historical data of switch transfer state. They used reinforcement learning to obtain the state transition constraints. The system they developed for the application of electric vehicles and the proposed motor control method was validated under 100 km acceleration in simulation. They didn't even consider the disturbance and load variation for checking the robustness of the proposed system.

Double MPC mothed is developed in the paper (X. Huang et al., 2020) to enhance the control performance and anti-interference performance of the PMSM drive system. The outer loop speed control is controlled by MPC to have better speed response and the inner loop current control is used a deadbeat predictive control strategy to avoid interference and to get better control performance. In order to testify to the proposed mothed the traditional MPC is compared with the proposed control strategy. And the proposed control has a better steady-state response, stronger anti-load disturbance performance, and faster dynamic response. As a limitation of this research works the application is not clearly specified.

In (Tan et al., 2020) present the MPC of interior permanent magnet synchronous motor (IPMSM) for electric vehicle applications. In this paper, a conventional control method (CCM) based MPC is developed for full-speed domain control. The authors assured the cascading MPC control strategy has a disadvantage in its limit of dynamic response performance of the motor and does not completely make use of the features of MPC's multi-objective simultaneous optimization. For this reason, they designed the non-cascading MPC in detail. From the simulation, the authors compared the cascade and non-cascade MPC with different load torque at different speed levels. Furthermore, for non-cascading MPC, the torque and speed responses are faster. As a gap, this study does not consider a constraint for the system.

The finite control set (FCS) based MPC controller is designed in (Murali et al., 2021) to control the speed of PMSM for the propulsion of EVs. The objective of this study was to enhance the dynamic response in the speed for a variety of EV driving circumstances. This was achieved by using the FCS-MPC algorithm and by comparing it with the classical field oriented control (FOC) strategy. The result gave an improved dynamic performance and better steady-state response for different speed conditions. For the control utilization, this study used the minimized square error type as a cost function.

In (Tian et al., 2023) an input-output feedback linearization is designed to optimize the cost function and formulate an improved linear predictive control method. The PMSM is highly nonlinear so it is very difficult to minimize the cost function of quadratic programming. This paper used the feedback linearization method to eliminate nonlinearity. But this is not further applicable in the practical realization. The control strategy is applied to IPMSM. The d and q-axis inductance are not equal. Because of this, these predictive controllers are unable to fully utilize the reluctance torque produced by the interaction of the unequal d-axis and q-axis inductance. Additionally, the predictive controllers must be improved in order to increase the torque-to-current ratio. This made complicated the control strategy and need the computation time of nonlinear model predictive control (NMPC) for practical implementation.

In (Mao et al., 2022) MPC based on a neural network for speed control of PMSM is presented in this paper. The main contribution of this research was by applying the fast gradient method (GM) decreased the computational cost and enhanced the response performance of the controller. This is suitable for a nonlinear model system. The speed predictive controller is based on particle swarm optimization-based echo state network (PSO-ESN) algorithm. But, the result shows about 0.9% overshoot occurred on the time response for different conditions.

In (Garcia et al., 2019) presented the modulated MPC for PMSM. The outer loop of speed control is used the deadbeat predictive control method to provide a quadrature current reference from the mechanical speed equation and the Kalman filter is used to estimate the load torque as a disturbance. The inner loop current control is used in the subsystem and MPC utilizes a cost function to find out the two active voltage vectors used for modulation control. The speed control gave good reference tracking and fast dynamic response. As a limitation of this work, the application of the system is not clearly specified and didn’t test for different variations.

In (Younesi et al., 2018) proposed the nonlinear MPC to control the speed of the PMSM. This paper described the demerit of the linear controller which is the limitation of the bandwidth, this is affected the inverter switching frequency. So, this research work stands to overcome this problem. The result delivered improved speed tracking and got inverter switching frequency 10 times lower. In the time response, the steady state error and settling time are good but the overshoot and undershoot occurred.

Most of the above researches did using d-q transformed dynamic model of PMSM. Even though, the system is naturally nonlinear and it is very difficult to get nominal points to linearize the motor. From the reviewed papers, some studies tried to linearize the full dynamic model of the motor by the only one operating point of the motor and then they designed a modulated controller. However, the operating point of the motor is depending on the characteristics of the speed and torque. In this thesis, as the speed equation is linear MPC applied to it as an outer loop control approach and the inner current loop controlled by GA based PI. The main advantage of MPC is it can consider a constraint on the system. In Table 2-2 presented the summary of the reviewed literatures shortly.

*Table 2-2: Summary of literature review*

| No. | Title | Authors | Method | Achievement | Gap |
|---|---|---|---|---|---|
| 1 | NMPC of PMSM with extra current constraint | (Tian et al., 2023) | NMPC with feedback linearization | -Avoiding the effect of external perturbation | The control strategy is complex, it needs large memory for implementation. |
| 2 | Improved NPMC speed control of PMSM | (Younesi et al., 2018) | NMPC compared with FOC | Minimizing the inverter switching frequency | Overshoot and undershoot occurred on the speed response |
| 3 | Speed control of PMSM based NN MPC | (Mao et al., 2022) | MPC based PSO-ESN | The computation time is decreased | About 0.9% overshoot occurred |

| | | | | | |
|---|---|---|---|---|---|
| 4 | Assessing finite control set based MPC speed control of PMSM for EVs | (Murali et al., 2021) | FCS-MPC algorithm | -Improved dynamic performance Compared with FOC and better SS response for different speed variation | Used minimized square error as cost function without considering constraints |
| 5 | Speed and current control of PMSM based on double MPC | (X. Huang et al., 2020) | MPC for outer loop control Deadbeat predictive control for inner loop | -Strong anti-load disturbance performance<br>-Fast dynamic response | Constraints are not considered |

**2.4. Overview of GA and PI Controller**

A proportional integral (PI) controller is a type of feedback control mechanism commonly used in control systems to regulate and stabilize a process. It is used the current error and the accumulated error over time to compute the control signal. The proportional control component of the PI responds to current error between the desire set point and the actual process value. The integral control component of the PI is considered the accumulated error over time. In this thesis, the PI controller used to control the inner loop of the system.

$$u(t) = k_p e(t) + k_i \int_0^t e(t)dt \tag{2.1}$$

GA is used to tune the gain parameters of PI controller. It is a stochastic adaptive search and optimization technique inspired by the process of natural selection and genetics(Oubelaid et al., 2022). The main idea behind a GA is to iteratively generate a population of potential solutions to a problem and apply genetic operation. i.e. selection, crossover and mutation to evolve and improve the solution over time.

## 2.5. Overview of LQR Controller

The LQR approach is an optimal control method that is used to control the linear system. It is a state feedback controller that selects the most effective control input using a quadratic cost function. Considering Equation (2.4) as a discrete time system, the cost function can be expressed as follows:

$$J = \sum_{k=0}^{M-1} (x^T(k)Qx(k) + u^T(k)Ru(k)) \tag{2.2}$$

Where, $Q$ and $R$ are a symmetric positive definite matrix, in order to get good dynamic performance for the system, the weight matrix must select appropriately.

The optimal control law is expressed as:

$$u = -Kx(k) \tag{2.3}$$

$K$ is the feedback gain of the optimal control

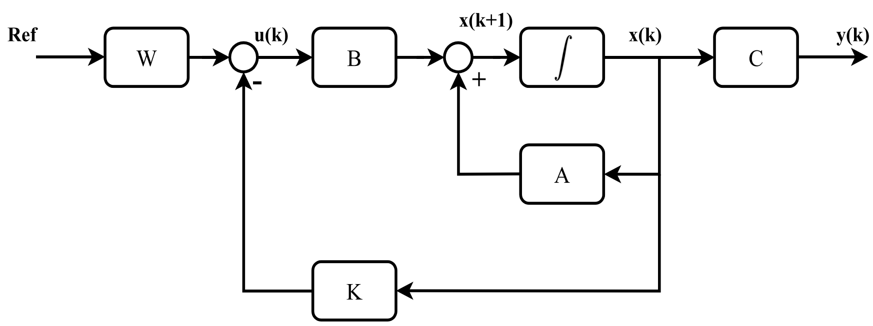


*Figure 2-8: Schematic diagram LQR controller [L6]*

## 2.6. Overview of MPC

MPC is an advanced approach used to control a system while satisfying a set of constraints. It is an optimal control that uses the current statues of the model and predicted the future behavior of the plant to take control action. MPC is based on iteration, finite window horizon of the plant model.

Let the discrete linear model of system is:

$$x(k+1) = Ax(k) + Bu(k)$$
$$y(k) = Cx(k) \tag{2.4}$$

With time step *k* state $x(k) \in R^m$, control input $u(k) \in R^n$, and *A* matrix $nxn$ ,B matrix $mxn$

The optimal control low is expressed as:

$$U = \arg\min_{U} J(x(k|k), U) \tag{2.5}$$

subject to $u^{\min} \leq u(k) \leq u^{\max}$

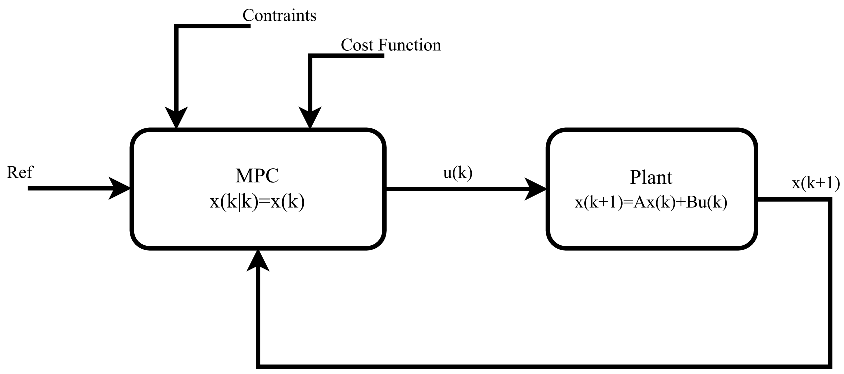


*Figure 2-9: Schematic diagram of MPC*

The optimization algorithm minimizes the cost function regarding to all predicted control inputs. *U* is the optimal solution for the control input series combined in one vector.

$$U = \left[ u(k|k) \quad u(k+1|k) \quad \ldots \quad u(k+H_c-1|k) \right]$$

Where, $H_c$ is control horizon commands the number of parameters used to capture the future control trajectory.

Prediction horizon means how far the future to be predicted or the length of moving horizon window. So, the optimal control obtained by minimizing the cost function within the optimization window.

# CHAPTER THREE

# 3. METHODOLOGY

## 3.1.Overview

In this chapter clearly explained the materials, methods and techniques used for the study. The analysis of vehicle dynamics, mathematical model of the PMSM drive, controller design, three phase inverter for PMSM, and their simulation are well performed in this section.

## 3.2.Materials

The high-level mathematical model package **MATLAB/Simulink 2021a** simulation software has been used to evaluate and verify the developed model. Equations and formulas have been also written properly by **MathType** software while **MS-Office 2019** used for document preparation and power points.

## 3.3.Methods

The work of this thesis is necessarily based on what has already been done by other related scholars. From the reviewed literatures relevant data are collected and analyzed. The mothed for this thesis work is expressed in the following Figure 3-1.

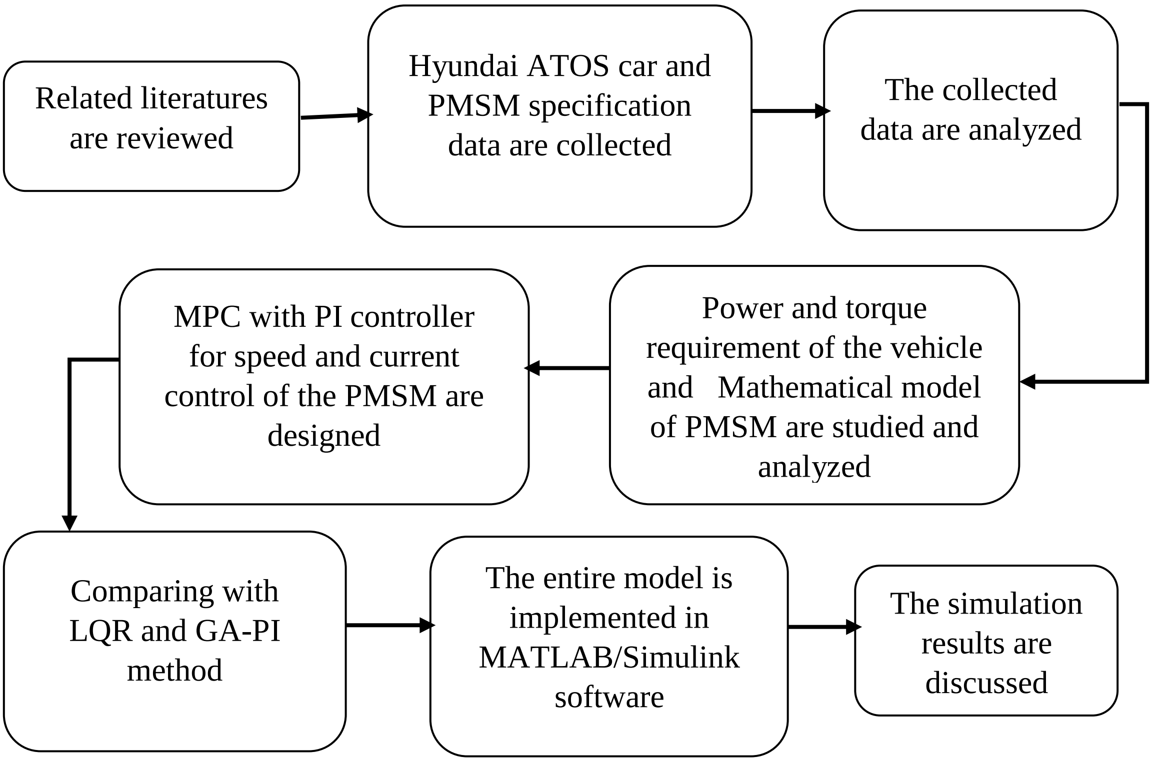


*Figure 3-1: Block diagram of the research methodology*

### 3.4.The Block Diagram of proposed PMSM drive for EV

The block diagram of the MPC based speed control of a PMSM drive for the propulsion of electric vehicle Hyundai ATOS car has shown in Figure 3-2. The difference error between the reference speed and measured speed is controlled by MPC. And the MPC could predict the current $I_q$ required from the system by using the speed measured value. In a vector control strategy, the d-axis $I_d$ represented the current flowing along the motor direct axis, which is aligned with the rotor magnetic field. When the PMSM is operating in a steady state, $I_d$ is usually set to zero. This is because the rotor magnetic field of a PMSM is generated by the permanent magnets and remains fixed with respect to the rotor. The control method regulated the q-axis current $I_q$ to control the motor torque. By manipulating the q-axis current, the control technique can regulate the motor speed and torque independently. Both PI current

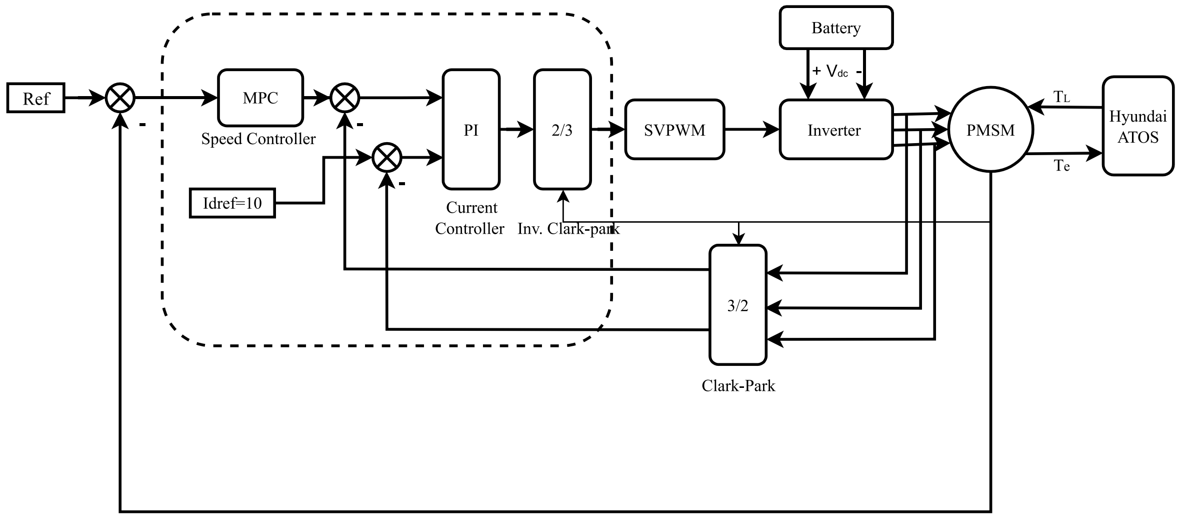


*Figure 3-2: Block diagram of the proposed control system*

control provides $V_{d-q}$ reference signal. SVPWM used the controller signal from PI controller as gate signal to generate the corresponding switching signal. The switching signal operates the six transistors for the process of three phase inverter to invert a supply DC to AC for the motor.

### 3.5.Electric Vehicle Dynamics

The electrical part of EVs are mainly consists of five components those are; electric motor, battery, power electronics, motor controller and battery controller. In order to determine the requirement of an EV traction system the road load for the vehicle is presented in this topic. The vehicle's free body diagram is shown in the Figure 3-3, clearly described the different forces acting on a vehicle. In the designing of the EV various parameters can be considered the rated speed of the motor (Akhtar et al., 2016).

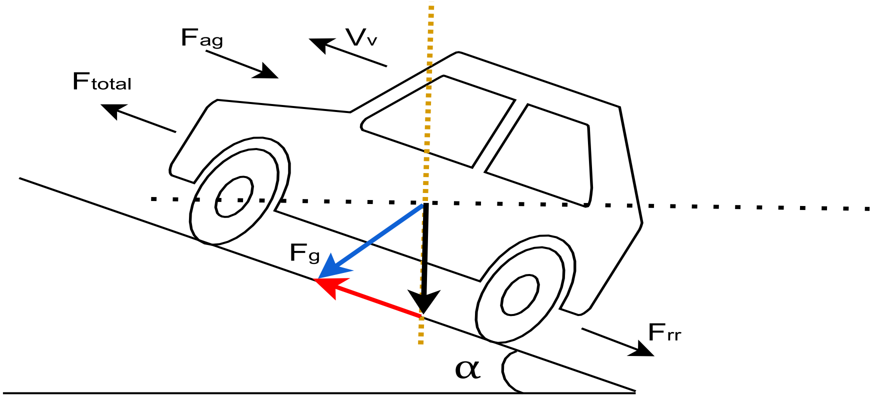


*Figure 3-3: Free body diagram of Hyundai ATOS vehicle*

### 3.5.1. Motive Force, Power and Torque of Hyundai ATOS Vehicle

Several forces are acting on the Hyundai ATOS vehicle under riding. In this thesis work the selection of the drive motor is according to the design specification of the vehicle dynamics. The model of the Hyundai ATOS vehicle dynamics considered road, wheel, and vehicle position. Forces are directly imposed on the vehicle when it is running on the road load as shown in Figure 3-3. The road load force includes the tire rolling force, aerodynamic drag force, and gradient force at the inclination surface. The total force is the sum of the below calculated three forces.

$$F_T = F_{rr} + F_{ad} + F_g \tag{3.1}$$

Where, $F_T$ is total force, $F_{rr}$ is rolling resistance force, $F_{ad}$ is aerodynamic drag force, and $F_g$ is gradient force.

Table 3-1: Hyundai ATOS car specification[L7]

| Parameter | Symbol | Value |
|---|---|---|
| Speed | $V_v$ | 100 kph |
| Gross weight | M | 1310 kg |
| Width | w | 1645 cm |
| Height | h | 1560 cm |
| Tire radius | r | 0.2 m |
| Coefficient of drag | $K_{ad}$ | 0.33 |
| Transmission gear ratio | $G_r$ | 4.4 |

The total force acting on the vehicle and the power requirement to overcome these forces are obtained as follows.

#### 3.5.1.1.Tire Rolling Resistance Force

This force is produced by the deformation of the tire as it makes a contact with the surface. The amount of rolling resistance depends on the weight of the vehicle, roughness of surface, and the position of the vehicle. According to (Vempalli et al., 2018)the equation of the rolling resistance force ( $F_{rr}$ ) is expressed as follows;

$$\begin{aligned} F_{rr} &= K_{rr} Mg\cos(\alpha) \\ &= 0.01\times1310\times9.81\times\cos(8) \\ &= 127.26N \end{aligned} \tag{3.2}$$

Where, $M$ is the gross mass of the Hyundai ATOS car, $g$ is the acceleration due to the gravity, $K_{rr}$ is the rolling resistance coefficient (concrete and asphalt on a good condition is considering for this study) and $\alpha$ is the inclination angle. The power ( $P_{rr}$ ) required to overcome the rolling resistance force is determined by:

$$\begin{aligned} P_{rr} &= F_{rr}V_v(\frac{m}{s}) \\ &= 127.26\times(\frac{100km}{3600s}) \\ &= 3.53kW \end{aligned} \tag{3.3}$$

Where, $V_v$ is the speed of the vehicle.

Table 3-2: Values of rolling resistance coefficient (S Chauhan et al.,2015)

| Contact Surface | $K_{rr}$ |
|---|---|
| Concrete(good/fair/poor) | 0.01/0.015/0.02 |
| Asphalt(good/fair/poor) | 0.01/0.017/0.022 |
| Macadam(good/fair/poor) | 0.015/0.022/0.037 |
| Mud(firm/medium/soft) | 0.037/0.09/0.15 |
| Sand(firm/soft/dune) | 0.06/0.15/0.3 |

#### 3.5.1.2. Aerodynamic drag Force

A vehicle moving through the air would experience aerodynamic drag, which opposes its speed. When a vehicle is in motion, it encounters resistance from the air pressure that it comes into contact with. It is basically produced from two components: skin friction and shape drag. Skin friction created from the friction between the air molecules and the surface of the vehicle. The pressure variations that result from the shape of the vehicle as it passes through the air created a shape drag. It is depending on speed, frontal area of the vehicle, drag coefficient and air density. According to (Workineh et al., 2021),(Vempalli et al., 2018) the equation of the aerodynamic drag force ( $F_{ad}$ ) is as follows:

$$\begin{aligned} F_{ad} &= \frac{1}{2} K_{ad} A_f \rho (V_v + v_a)^2 \\ &= \frac{1}{2} \times 0.33 \times 2.18 \times 1.23 \times (\frac{100km}{3600} + 0)^2 \\ &= 341.4N \end{aligned} \tag{3.4}$$

Where,

$K_{ad}$ - coefficient of aerodynamic drag (its value is 0.33 from the vehicle specification).

$A_f$ - frontal area of the vehicle calculated by $Af = 0.85 \times h \times w = 0.85 \times 1.56 \times 1.64 = 2.18m^2$

$h$ and $w$ - are the height and width of the vehicle respectively

$v_a$ - speed of air assumed to be zero.

$\rho$ - the air density in $\frac{kg}{m^3} = 1.23$

When developing the dynamics of a Hyundai ATOS electric vehicle, there are additional forces to consider, including aerodynamic lift force. The above two aerodynamic forces to overcome, the power requirement usually considered as a maximum of 1.5kW (Minyamer Gelawe, 2020)

#### 3.5.1.3.Gradient (Climbing) Resistance Force

The force needed for a vehicle to climb up or down a slope is referred to as the gradient climbing force. The vehicle must overcome the force of gravity when climbing a slope. The force required to overcome this gravitational force is the gradient force ( $F_g$ ) (Atamnia et al., 2020). In this thesis the vehicle performance analysis, only the uphill climbing is considered. Both the weight of the vehicle and the angle of the slope are factors in determining this force.

$$\begin{aligned} F_g &= Mg \sin(\alpha) \\ &= 1310 \times 9.81 \times \sin(8) \\ &= 1788.5N \end{aligned} \tag{3.5}$$

The climbing power ( $P_c$ ) of the vehicle to overcome the gradient force determined by:

$$\begin{aligned} P_c &= F_g v_c \\ &= 1788.5 \times (\frac{50km}{3600s}) \\ &= 24.84kW \end{aligned} \tag{3.6}$$

Where, $v_c$ is climbing velocity, its value is half of the maximum speed of the vehicle.

Then, the required maximum power of PMSM drive to propel Hyundai ATOS vehicle is the total tractive power calculated below.

$$\begin{aligned} P_{total} &= P_{rr} + P_{ad} + P_g \\ &= 3.53 + 1.5 + 24.84 \\ &= 29.87kW \end{aligned} \tag{3.7}$$

From the equation the total force acting on Hyundai ATOS vehicle will be:

$$\begin{aligned} F_T &= F_{rr} + F_{ad} + F_g \\ &= 127.26 + 341.4 + 1788.5 \\ &= 2257.16N \end{aligned} \tag{3.8}$$

In addition, the losses result from the transmission of power to the vehicle's wheel must also be considered(Workineh et al., 2021). So, the mechanical power output ( $MP_{peak}$ ) on the wheel is given by:

$$\begin{aligned} MP_{peak} &= \frac{P_{total}}{\eta_g} \\ &= \frac{29.87}{0.98} = 30.5kW \end{aligned} \tag{3.9}$$

To propel the vehicle the motor drive can be select up to 35kW maximum power. This information is used to select the PMSM parameters.

Figure 3-4 shown the total motive force along with each component of the force acting on the Hyundai ATOS vehicle comparing with the angle approach. By assuming that the air velocity is zero, and the vehicle is moving on uphill (8 degree approaching angle) at a speed of 50 km/h. the aerodynamic drag force and the rolling resistance force remaining constant when the approaching angle increases. But the gradient force is increases linearly with approaching angle.

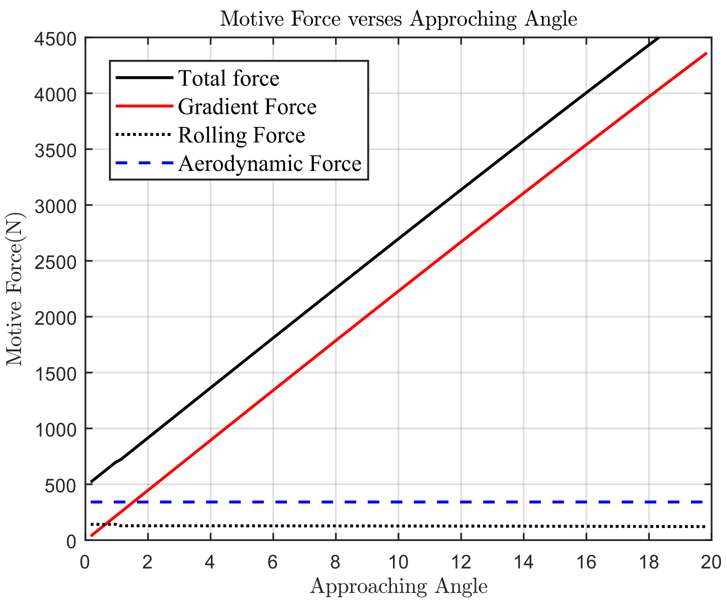


*Figure 3-4: Motive forces verses approaching angle*

In Figure 3-5 shown the characteristics between power consumption to propel the vehicle and the speed of vehicle. If the speed of the vehicle is increasing the power consumption also respectively increases. The vehicle can move at the maximum speed with the power consumption 30kW. In order to model the motor, it is also important to determine the rated torque and maximum torque of the motor requirement.

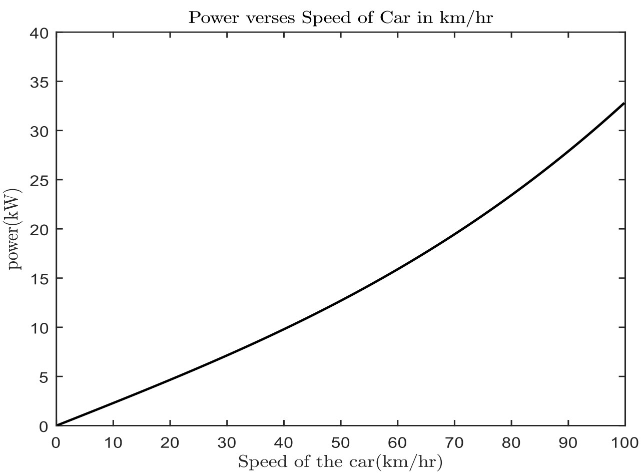


*Figure 3-5: Desire total power verses speed of car in kph*

#### 3.5.1.4.Torque required on the drive wheel

It is a crucial to calculate the torque on the drive wheel in order to get the required drive characteristics. As considering 89% overall transmission efficiency of the vehicle the actual torque load is calculated as follow:

$$\begin{aligned} T_{load} &= \frac{P_{total}}{\omega_m}\eta \\ &= \frac{30.1kW}{314\, rad/s} \times 0.89 \\ &= 85.3Nm \end{aligned} \tag{3.10}$$

Where, $T_{load}$ is the actual torque rate, $\omega_m$ is rated speed of the motor from Table 3.3, and $\eta$ is the transmission efficiency.

According (Workineh et al., 2021) to obtain the torque on the drive wheel can be used the following equation:

$$\begin{aligned} T_w &= F_T \times \frac{r}{G_r} \\ &= 2257.16 \times \frac{0.2}{4.4} \approx 103Nm \end{aligned} \tag{3.11}$$

Where $T_w$ is torque on the drive wheel, $F_T$ is total force, $r$ is radius of the wheel, and $G_r$ is gear ratio. Values for $r$ and $G_r$ are taken from the specification of the vehicle listed in Table 3-1. Therefore, the Hyundai ATOS car can be ride with 35 kW power and 85.3 Nm torque of electric motor at 314 rad/s and has to generate 103 Nm of torque on the drive wheel of the vehicle.

Table 3-3: PMSM parameter specification

| Parameter | Symbol | Value |
|---|---|---|
| Power rated | P | 35kW |
| Speed rated | $\omega_m$ | 314 rad/s |
| Toque rated | Te | 111 Nm |
| Torque max | Tmax | 126 Nm |
| Stator resistance | Rs | 0.05 ohm |
| Inductance d-q axis | $L_d$,$L_q$ | $6.35\times10^{-4}$ mH |
| Flux magnet | $\lambda_m$ | 0.192 Wb |
| Moment of inertia | J | 0.011 kg.$m^2$ |
| Viscous dimpling | B | 0.002 Ns/m |
| Pole pair | p | 4 |

### 3.6. Mathematical Model of PMSM drive

A two-phase motor in the d-q coordinate system is applied to derive the dynamic model of the PMSM. This method is necessary because of the conceptual easiness/simplicity it have. The mathematical model is obtained from one set of two windings on the stator as the rotor has only a magnet. This process is adopted using reference frame transformation method.

#### 3.6.1. Reference Frame Transformation

Reference frame is a great observer platform. Each platform gives a unique view of the system and a clear explanation of the system equations. If the three and two phases are shown to be equivalent in outcome, a dynamic model for the three-phase PMSM can be developed the two-phase motor. The MMF produced in the two-phase and three-phase windings are equal, and the current magnitudes are identical, which forms the basis for the equivalence. Since the three-phase winding is assumed to have N turns per phase and equal current magnitudes, the two-phase windings will have 3N/2 turns per phase for MMF equality as shown in Figure 3-7.

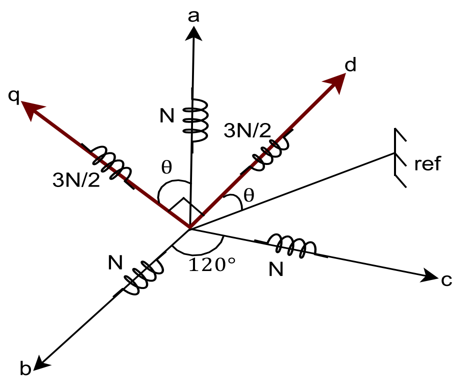


*Figure 3-6: Three and two-phase stator winding*

The three-phase to two-phase transformation usually based on the following assumptions:

- Eddy current and hysteresis current losses are negligible
- Rotor flux is concentrated across d-axis and zero along q-axis.

The way to transform from three phase plan to the reference two phase fixed plane is called Clarke transform and the reverse is inverse Clarke transform.

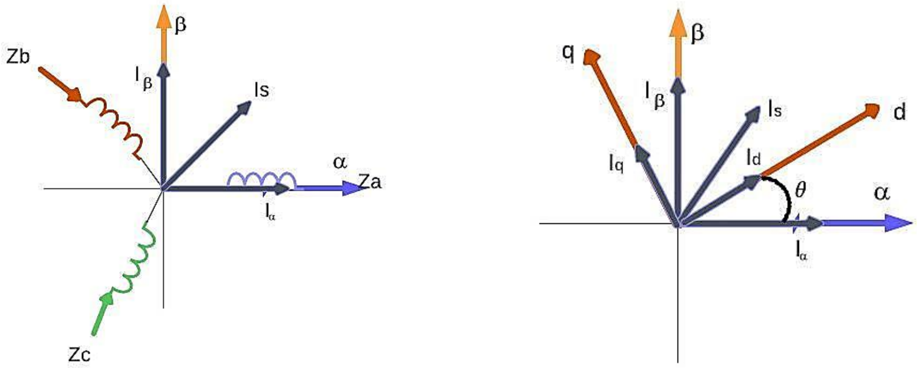


*Figure 3-7: Clarke-Park transformation*

$$\begin{bmatrix} z_\alpha \\ z_\beta \\ z_0 \end{bmatrix} = \frac{2}{3} \begin{bmatrix} 1 & -\frac{1}{2} & -\frac{1}{2} \\ 0 & \frac{\sqrt{3}}{2} & -\frac{\sqrt{3}}{2} \\ \frac{1}{2} & \frac{1}{2} & \frac{1}{2} \end{bmatrix} \begin{bmatrix} z_a \\ z_b \\ z_c \end{bmatrix} \tag{3.12}$$

$$\begin{bmatrix} z_a \\ z_b \\ z_c \end{bmatrix} = \frac{2}{3} \begin{bmatrix} 1 & 0 & 0 \\ -\frac{1}{2} & \frac{\sqrt{3}}{2} & 0 \\ -\frac{1}{2} & -\frac{\sqrt{3}}{2} & 0 \end{bmatrix} \begin{bmatrix} z_\alpha \\ z_\beta \\ z_0 \end{bmatrix} \tag{3.13}$$

Equation (3.12) and (3.13) are illustrated for Clarke transform and inverse transform respectively, where the symbol *z* represented and valid for current and voltage variable.

The way to convert from two-phase fixed reference plane perpendicular to each other at $90^0$ to two-phase rotating rotor plane is called park transform and the reverse is inverse park transform.

$$\begin{bmatrix} z_d \\ z_q \end{bmatrix} = \begin{bmatrix} \cos\theta_r & \sin\theta_r \\ -\sin\theta_r & \cos\theta_r \end{bmatrix} \begin{bmatrix} z_\alpha \\ z_\beta \end{bmatrix} \tag{3.14}$$

$$\begin{bmatrix} z_\alpha \\ z_\beta \end{bmatrix} = \begin{bmatrix} \cos\theta_r & -\sin\theta_r \\ \sin\theta_r & \cos\theta_r \end{bmatrix} \begin{bmatrix} z_d \\ z_q \end{bmatrix} \tag{3.15}$$

Equation (3.14) and (3.15) are expressed for park transform and inverse Park transform respectively, where $\theta_r$ is the rotor angle. Hence, the current and voltage variables of the d-q phasor components can be determined using the above equations.

### 3.6.2. Three-phase Equivalent Circuit of PMSM

The three phase PMSM can be expressed by an equivalent circuit that contains a rotor circuit and a stator circuit. As shown in the Figure 3-9, the three phase AC power supply is connected to the stator circuit, while the permanent magnet is connected to the rotor circuit. the three-phase equivalent circuit of a PMSM can expressed as follows:

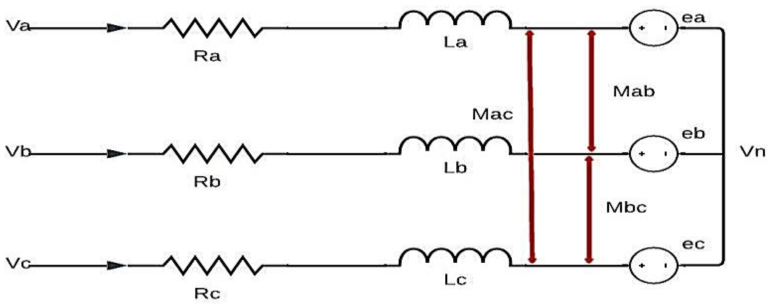


*Figure 3-8: Stator circuit of a PMSM*

The stator circuit of a PMSM contains, three phase voltage source and three phase stator winding. According to the three-phase voltage source applied to the PMSM is expressed as follows:

$$V_a = V_p \sin \omega_r t$$
$$V_b = V_p \sin(\omega_r t - \frac{2\pi}{3}) \tag{3.16}$$
$$V_c = V_p \sin(\omega_r t + \frac{2\pi}{3})$$

If a self-inductance, mutual inductance and stator resistance assumed equal, therefore;

$$R_a = R_b = R_c = R_s$$
$$L_a = L_b = L_c = L \tag{3.17}$$
$$M_{ab} = M_{bc} = M_{ac} = M$$

In this circuit, $R_s$ is stator resistance, $L$ is stator inductance, and $M$ is mutual inductance. The PMSM drives by generating a rotating magnetic field in the stator, which cooperates with the permanent magnet in the rotor. The interaction between the magnetic field outcomes in the rotation of the rotor. The equivalent circuit can be used to study the performance of the PMSM under different conditions as well as to design control strategies for the motor.

### 3.6.3. Model and dq0 Equivalent Circuit of PMSM

The dq0 equivalent circuit of a PMSM is a transformation of the three-phase equivalent into a two-axis reference plane using park transformation.

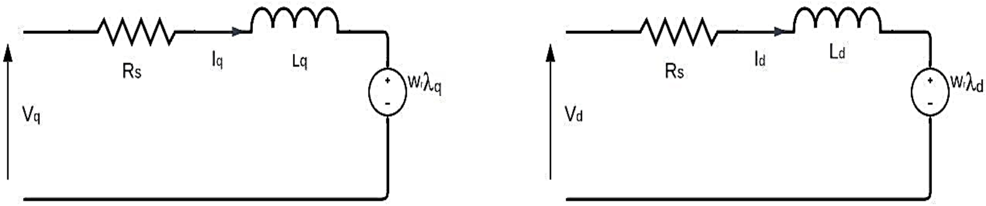


*Figure 3-9: PMSM d-q axis equivalent circuit*

This reference plane involves two perpendicular coordinates, these are; the d-axis aligned with the permanent magnet flux, and the q-axis, which is perpendicular to the d-axis.

From Equation (3.12) and (14) the dq0 equivalent circuit can be derived to stator q-axis and d-axis as illustrated in Figure 3-10 (Chai et al., 2013).

$$V_d = R_s I_d + \frac{d}{dt}\lambda_d - \omega_r \lambda_q \quad (3.18)$$

$$V_q = R_s I_q + \frac{d}{dt}\lambda_q + \omega_r \lambda_d \quad (3.19)$$

Where, $V_d$ and $V_q$ are d-q axis voltages, $I_d$ and $I_q$ are d-q axis currents, and $\lambda_d$ and $\lambda_q$ are d-q axis flux linkage.

The d-q axis flux linkages are expressed by:

$$\lambda_d = L_d I_d + \lambda_m \quad (3.20)$$

$$\lambda_q = L_q I_q \quad (3.21)$$

Where, $L_d$ and $L_q$ are d-q axis inductances, and $\lambda_m$ is the permanent magnet flux linkage.

As substituting Equation (3.20) and (3.21) into Equation (3.18) and (3.19), it becomes:

$$V_d = R_s I_d + L_d \frac{d}{dt} I_d - L_q \omega_r I_q \quad (3.22)$$

$$V_q = R_s I_q + L_q \frac{d}{dt} I_q + L_d \omega_r I_d + \omega_r \lambda_m \quad (3.23)$$

According to (X. Huang et al., 2020) and (G. Huang et al., 2022) the electromagnetic torque equation is expressed as:

$$T_e = \frac{3}{2} p(\lambda_m I_q + (L_d - L_q) I_d I_q) \tag{3.24}$$

And the mechanical torque equation is:

$$J \frac{d\omega_m}{dt} = T_e - b\omega_m - T_L \tag{3.25}$$

Where, $T_e$ is electromagnetic torque, $T_L$ is torque load, $J$ is moment of inertia, $p$ is pole pair, $b$ is the damping coefficient, and $\omega_m$ is mechanical speed.

Since,

$$\omega_r = p\omega_m \tag{3.26}$$

In this thesis surface mounted PMSM is selected. Hence, the d-axis inductance and q-axis inductance is equal ( $L_d = L_q = L$ ). Therefore, the simplified electromagnetic torque is given by:

$$T_e = \frac{3}{2} p\lambda_m I_q \tag{3.27}$$

Rearranging Equation (3.22) and (3.23)

$$\frac{dI_d}{dt} = -\frac{R_s}{L} I_d + \omega_r I_q + \frac{1}{L} V_d \tag{3.28}$$

$$\frac{dI_q}{dt} = -\frac{R_s}{L} I_q - \omega_r I_d - \frac{\lambda_m}{L} \omega_r + \frac{1}{L} V_q \tag{3.29}$$

Substituting Equation (3.26) and (3.27) into Equation (3.25)

$$\frac{J}{p} \frac{d\omega_r}{dt} = \frac{3}{2} p\lambda_m I_q - \frac{b}{p} \omega_r - T_L \tag{3.30}$$

$$\frac{d\omega_r}{dt} = \frac{3p^2}{2J} \lambda_m I_q - \frac{b}{J} \omega_r - \frac{p}{J} T_L \tag{3.31}$$

### 3.6.4. State Space Model of a PMSM

The d-q model of a PMSM Equation (3.28), (3.29) and (3.31) can be expressed in state space model as follows:

Define $x_1 = I_d, x_2 = I_q, x_3 = \omega_r$

$$\begin{aligned} \dot{x}_1 &= -\frac{R_s}{L} x_1 + x_2 x_3 + \frac{1}{L} V_d \\ \dot{x}_2 &= -\frac{R_s}{L} x_2 - x_1 x_3 - \frac{\lambda_m}{L} x_3 + \frac{1}{L} V_q \\ \dot{x}_3 &= \frac{3p^2}{2J} \lambda_m x_2 - \frac{b}{J} x_3 - \frac{p}{J} T_L \end{aligned} \tag{3.32}$$

However, the dynamic model of the motor is highly nonlinear. The nonlinearity occurred on both of current equations. Unfortunately, it is very difficult to obtain nominal points of the motor. In this thesis, decided to use linear MPC to control the speed of the motor as an outer loop as the speed equation is linear, and GA based PI used to control d-q current as an inner loop.

### 3.7. Space Vector Pulse Width Modulation (SVPWM)

SVPWM is a method used to control the output voltage of a three-phase inverter by regulating the duty cycles of the PWM signals. In EVs propulsion, the AC motor drive is fed from three phase inverter with a source Li-ion battery. SVPWM is in charge for creating PWM signals to operate an inverter's switches, which then generates the essential modulated voltage to drive the motor at the desired speed or torque. The SVPWM approach has the following advantages (in & 2015):

- Produces sinusoidal output voltage with low harmonics distortion
- Reduced switching losses

A three-phase inverter as shown the equivalent circuit in the figure, it converts a DC supply to a three output legs using six switches (transistors), which could be connected to a three-phase PMSM.

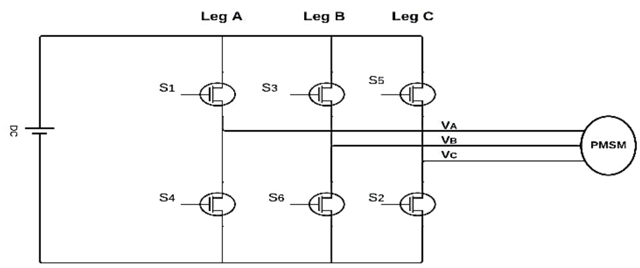


*Figure 3-10: Three-phase inverter*

There are eight possible switching configurations. The voltage that is applied to the motor terminals depends on these switching configurations. Table 3-3 lists eight possible switching states (Y. Huang et al., 2020). According to the switching order, the positions of the three switches determined by each of those eight states. The output voltage can be obtained by ON and OFF states of the upper switches $S_1$, $S_3$ and $S_5$.

*Table 3-4: Eight possible switching states*

| Space vector | $S_1$ | $S_3$ | $S_5$ |
|---|---|---|---|
| $V_0$ | 0 | 0 | 0 |
| $V_1$ | 0 | 0 | 1 |
| $V_2$ | 0 | 1 | 0 |
| $V_3$ | 0 | 1 | 1 |
| $V_4$ | 1 | 0 | 0 |
| $V_5$ | 1 | 0 | 1 |
| $V_6$ | 1 | 1 | 0 |
| $V_7$ | 1 | 1 | 1 |

The PWM algorithm controls based on the switching space vectors ($V_0$-$V_7$). The six-output vector are non-zero values separated by $60^0$ and the remains two vectors are null as shown in Figure 3-11.

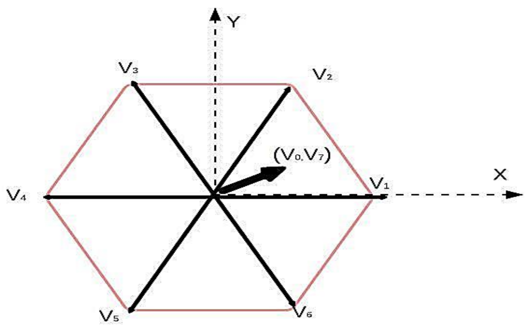


*Figure 3-11: Space vector hexagon with basic voltage vector*

In order to create a constant rotating space vector, the SVPWM technique aim is to produce switching sequences that match the reference voltage vector for the result every PWM period ($T_p$) ON time duration of pulses. Considering Figure 3-12 which is a projected view of sector 1 in Figure 3-11 to synthesize the desired voltage vector ($V_{out}$). This is accomplished by using $V_1$ for a time required ($T_1$), $V_2$ for a time required ($T_2$), and zero vector for the amount of time required ($T_0$) to give a resultant vector $V_{out}$.

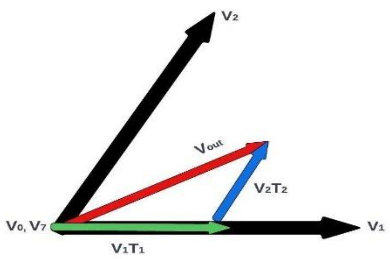


*Figure 3-12: Output voltage as adjacent vector in sector 1*

Time duration of T0, T1, and T2 can be obtained by the following equations:

$$T_1 = \left| \frac{V_{out}}{V_1} \right| T_p \tag{3.33}$$

$$T_2 = \left| \frac{V_{out}}{V_2} \right| T_p \tag{3.34}$$

$$T_0 = T_p - (T_1 + T_2) \tag{3.35}$$

The resultant voltage ($V_{out}$) can then be calculated as:

$$V_{out} = V_1 T_1 + V_2 T_2 + V_0 T_0 \tag{3.36}$$

Where $T_p$ is PWM period

Therefore, the switching time for sector 1(adjacent vector $V_1$ and V2) is $V_0$ -$V_1$ -$V_2$ -$V_7$ -$V_7$ -$V_2$ - $V_1$ -$V_0$.

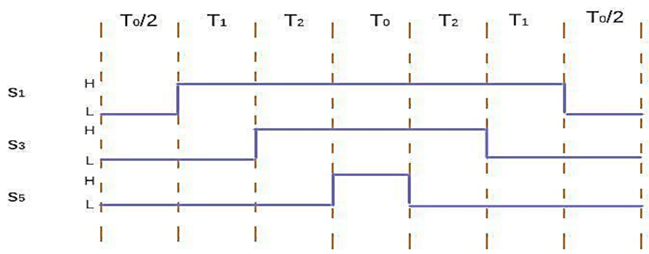


*Figure 3-13: Switching time for sector 1*

According to the switching statues for other sectors is performed through this procedure.

# CHAPTER FOUR

# 4. CONTROLLER DESIGN

## 4.1. Current Inner Loop PI controller

PI controller is employed for inner loop of the PMSM to control the current to correct the error between the measured and desired current $I_{dq}$. The gain parameters are tuned by using GA technique.

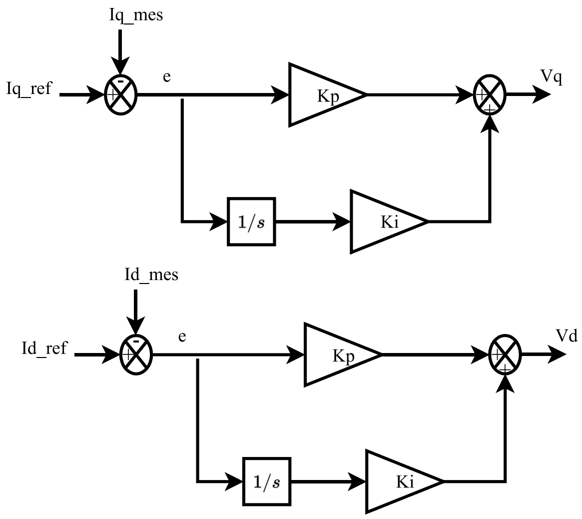


*Figure 4-1: PI current controller*

$$V_q = k_p e(t) + k_i \int_0^t e(t)dt$$
$$V_d = k_p e(t) + k_i \int_0^t e(t)dt \qquad (4.1)$$

## 4.2. Speed Outer Loop PI Controller

PI control is also used for the outer loop to control the speed of the motor to compare with the proposed MPC strategy. The controller is used to compensate the error from the difference of the measured and the desired speed of the motor. The gain parameters are tuned using GA technique.

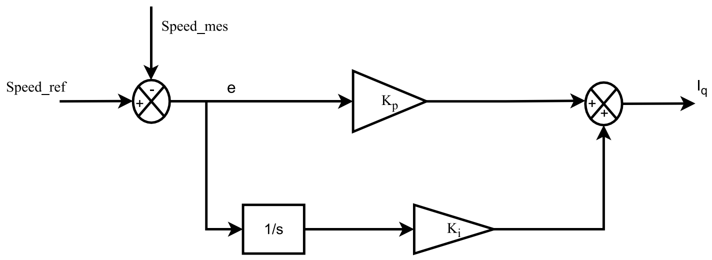


*Figure 4-2: PI speed controller*

$$I_q = k_p e(t) + k_i \int_0^t e(t)dt \tag{4.2}$$

### 4.3. Speed Outer Loop LQR Controller

In this thesis, LQR control approach provides for comparison to compare with the proposed MPC. The LQR is an optimal control theory for a linear system. From the given of a PMSM model the speed Equation (3.31) is linear. LQR is designed to minimize a cost function that combines the system state variable and control input. By minimizing the cost function, the controller would stabilize the system while achieving the desired performance. From Equation (4.8) discretized model, the cost function is given by:

$$J = \sum_{k=0}^{p-1} x(k)^T W x(k) + v(k)^T R v(k) \tag{4.3}$$

Where, $W$ and $R$ are a positive definite weighting matrix of state variable and control input respectively. The weighting matrix are tuned by using GA methods to get the optimal values.

If $\lambda$ is a Lagrange multiplier, the Hamiltonian formulation is expressed by:

$$H = \frac{1}{2}(x(k)^T W x(k) + v(k)^T R v(k)) + \lambda(k)^T (A_d x(k) + B_d v(k)) \tag{4.4}$$

From the above formulation the necessary conditions are:

$$x(k+1) = \frac{\partial H}{\partial \lambda} = A_d x(k) + B_d v(k)$$
$$\lambda(k+1) = \frac{\partial H}{\partial x} = W x(k) + A_d^T \lambda(k)$$
$$0 = \frac{\partial H}{\partial v} = Rv + B_d^T \lambda(k)$$

Then, the control input is derived as: $v = -R^{-1} B_d^T \lambda(k)$

By taking the algebraic riccati Equation (4.5), the Lagrange multiplier becomes:

$$A_d^T P + P A_d - P B_d R^T B_d^T P + W = 0 \tag{4.5}$$

$$\lambda(k) = P x(k) \tag{4.6}$$

The control law is expressed in the following form:

$$v = -K x(k) \tag{4.7}$$

Where, $K = R^{-1}B_d^T P$ is the gain of LQR control algorithm

As mentioned in previous topic, the control signal from the outer loop controller is a reference to current controller ( $I_q$ ).

### 4.4. Speed Outer Loop MPC Controller

From the given dynamic model of the PMSM, the speed equation is a linear. As outer loop control technique the speed can be controlled apart. So, the speed Equation (3.31) can be discretized using Forward-Euler method by considering sampling period ( $T_{sw}$ ) for the speed loop as follows:

$$\begin{aligned} \omega_r(k+1) &= (1-\frac{T_{sw}b}{J})\omega_r(k) + \frac{3p^2T_{sw}\lambda_m}{2J}I_q(k) - \frac{T_{sw}p}{J}T_L \\ &= A_d\omega_r(k) + B_dI_q(k) + d_\varepsilon \end{aligned} \tag{4.8}$$

Where, $A_d = \left(1-\frac{T_{sw}b}{J}\right), B_d = \frac{3p^2T_{sw}\lambda_m}{2J}, d_\varepsilon = -\frac{T_{sw}pT_L}{J}$

Defining; $x(k) = \omega_r$ and $v(k) = I_q$

$$\begin{aligned} x(k+1) &= A_d x(k) + B_d v(k) + d_\varepsilon \\ y(k) &= C_d x(k) \end{aligned} \tag{4.9}$$

In Equation (4.9) considering $x(k)$ and $v(k)$ as the state and control input of the model respectively. The disturbance $d_\varepsilon$ from the equation is eliminated to formulate MPC. According to the current state and the input from the control, the dynamic model in MPC is used to forecast the future behavior. The system's desired performance is quantified by a cost function that is optimized using these predictions. By Assuming;

$$\Delta x(k) = x(k) - x(k-1) \tag{4.10}$$

$$\Delta v(k) = v(k) - v(k-1) \tag{4.11}$$

The new state variable vector is defined as $X(k) = \left[\Delta x(k) \quad y(k)\right]^T$. Note that the control input to the new state space model is $\Delta v(k)$. So, the incremental predictive model can be expressed as follows;

$$X(k+1) = \tilde{A}X(k) + \tilde{B}\Delta v(k)$$
$$y(k) = \tilde{C}X(k) \tag{4.12}$$

Where, $\tilde{A} = \begin{bmatrix} A_d & o^T \\ C_d A_d & 1 \end{bmatrix}, \tilde{B} = \begin{bmatrix} B_d \\ C_d B_d \end{bmatrix}$ and $\tilde{C} = \begin{bmatrix} 0 & 1 \end{bmatrix}$ these are called an augmented matrix, which will be used in the design of predictive control.

Based on the formulation of the augmented state space model, the next phase in the design of a predictive control system is to compute the predicted plant output with the future control signal. This prediction is expressed within an optimization window. Assume the current moment is $k$ and the state variable can be measurable in this time. Then, the future state variable and the future control trajectory are denoted by:

$$\begin{bmatrix} X(k+1|k) & X(k+2|k) & \dots & X(k+H_p|k) \end{bmatrix}$$
$$\begin{bmatrix} \Delta v(k) & \Delta v(k+1) & \dots & \Delta v(k+H_c-1) \end{bmatrix}$$

Where, $H_p$ is prediction horizon which is the length of the optimization window, $H_c$ is control horizon which gives the parameters used to capture the future control signal. Then the future state variable can be calculated as follows:

$$\begin{aligned} X(k+1|k) &= \tilde{A}X(k) + \tilde{B}\Delta v(k) \\ X(k+2|k) &= \tilde{A}X(k+1) + \tilde{B}\Delta v(k+1) \\ &= \tilde{A}^2 X(k) + \tilde{A}\tilde{B}\Delta v(k) + \tilde{B}\Delta v(k+1) \\ &\vdots \\ X(k+H_p|k) &= \tilde{A}^{H_p} X(k) + \tilde{A}^{H_p-1}\tilde{B}\Delta v(k) + \ldots + \tilde{A}^{H_p-H_c}\tilde{B}\Delta v(k+H_c-1) \end{aligned} \tag{4.13}$$

From the predicted state variables, the predictive output variables are:

$$\begin{aligned} y(k+1|k) &= \tilde{C}X(k+1) = \tilde{C}\tilde{A}X(k) + \tilde{C}\tilde{B}\Delta v(k) \\ y(k+2|k) &= \tilde{C}X(k+2) = \tilde{C}\tilde{A}^2 X(k) + \tilde{C}\tilde{A}\tilde{B}\Delta v(k) + \tilde{C}\tilde{B}\Delta v(k+1) \\ &\vdots \\ y(k+H_P|k) &= \tilde{C}\tilde{A}^{H_p} X(k) + \tilde{C}\tilde{A}^{H_p-1}\tilde{B}\Delta v(k) + \cdots + \tilde{C}\tilde{A}^{H_p-N_c}\tilde{B}\Delta v(k+H_c-1) \end{aligned} \tag{4.14}$$

The predictive output variable is expressed by present time state variable $X(k)$ and future control variables. Equation (4.14) can be transformed into matrix form as follows:

$$Y = EX(k) + Q\Delta V \tag{4.15}$$

Where, $$E=\begin{bmatrix}\tilde{C}\tilde{A}\\ \tilde{C}\tilde{A}^2\\ \vdots\\ \tilde{C}\tilde{A}^{H_p-1}\end{bmatrix},Q=\begin{bmatrix}\tilde{C}\tilde{B} & 0 & \cdots & 0\\ \tilde{C}\tilde{A}\tilde{B} & \tilde{C}\tilde{B} & \cdots & 0\\ \vdots & \vdots & \ddots & \vdots\\ \tilde{C}\tilde{A}^{H_p-1}\tilde{B} & \tilde{C}\tilde{A}^{H_p-2}\tilde{B} & \cdots & \tilde{C}\tilde{A}^{H_p-H_c}\tilde{B}\end{bmatrix}$$

$$Y=\left[y(k+1\,|\,k)\quad y(k+2\,|\,k)\quad \cdots \quad y(k+H_P\,|\,k)\right]^T$$
$$\Delta V=\left[\Delta v(k)\quad \Delta v(k+1)\quad \cdots \quad \Delta v(k+H_c-1)\right]^T$$

For the given speed set point $s_{ref}(k)$ at current time *k*, within the prediction horizon the goal of the predictive control system is to get the predicted output as close as possible to the reference signal. Vector $Y$ contains the incremental output variables up to the length of prediction horizon and vector $\Delta V$ contains the incremental the rate of change of control signal up to the length of control horizon. $\Delta V$ is called an optimal solution or decision variable. The procedure is followed the receding horizon control law that means, from the optimal parameter vector $\Delta V$ the control variable is implement the first sequence. By assuming the set point information presented in the data vector $S_r$ to define the cost function.

$$S_r=\Big[\overbrace{1\quad 1\quad \cdots \quad 1}^{H_p}\Big]s_{ref}(k) \tag{4.16}$$

Therefore, the cost function $J$ can be chosen as:

$$J=\frac{1}{2}\left(Y-S_r\right)^T\bar{Q}\left(Y-S_r\right)+\frac{1}{2}\Delta V^T R\Delta V \tag{4.17}$$

Where the first term is the error minimization between the set point and the predicted output and the second term is the control parameter vector to make the cost function as small as possible, with $\bar{Q}$ and *R* are the positive definite diagonal matrix as a tuning parameter. The $\bar{Q}$ and *R* are tuned by using GA technique to get the optimal values.

By substituting Equation (4.16) into Equation (4.17), *J* can be expressed as:

$$\begin{aligned}J&=\frac{1}{2}(EX(k)+Q\Delta V-S_r)^T\bar{Q}(EX(k)+Q\Delta V-S_r)+\frac{1}{2}\Delta V^T R\Delta V\\ &=\frac{1}{2}(EX(k)-S_r)^T\bar{Q}(EX(k)-S_r)+\frac{1}{2}\Delta V^T[\bar{Q}^T Q\bar{Q}+R]\Delta V\\ &\quad+\Delta V^T\bar{Q}^T Q(EX(k)-S_r)\end{aligned} \tag{4.18}$$

### 4.4.1. Constraint on Control Input

The constraints are defined to ensure the system operation within desire boundaries and to satisfy a specific requirement. The control variable of the plant quadrature current defined as $v(k)$ can be formulated the inequality constraint as:

$$v^{\min} \leq v(k) \leq v^{\max} \tag{4.19}$$

$v(k)$ is an incremental variable at $k$ moment. It can express by two inequities:

$$v(k) \leq v^{\max} \tag{4.20}$$

$$-v(k) \leq -v^{\min} \tag{4.21}$$

By rearranging and substituting Equation (3.46) in to (3.55) and (3.56)

$$\begin{aligned}
&\Delta v(k) + v(k-1) \leq v^{\max} \\
&\Delta v(k) \leq v^{\max} - v(k-1) \\
&-\Delta v(k) - v(k-1) \leq -v^{\min} \\
&-\Delta v(k) \leq -v^{\min} + v(k-1)
\end{aligned}$$

In matrix form, it becomes:

$$\begin{bmatrix} 1 \\ -1 \end{bmatrix} \Delta v(k) \leq \begin{bmatrix} v^{\max} - v(k-1) \\ -v^{\min} + v(k-1) \end{bmatrix} \tag{4.22}$$

The next incremental variable at *k+1* moment is

$$\begin{aligned}
&v(k+1) \leq v^{\max} \\
&\Delta v(k+1) + v(k) \leq v^{\max} \\
&\Delta v(k+1) + \Delta v(k) + v(k-1) \leq v^{\max} \\
&\Delta v(k+1) + \Delta v(k) \leq v^{\max} - v(k-1)
\end{aligned}$$

$$\begin{aligned}
&-v(k+1) \leq -v^{\min} \\
&-\Delta v(k+1) - v(k) \leq -v^{\min} \\
&-\Delta v(k+1) - \Delta v(k) - v(k-1) \leq -v^{\min} \\
&-\Delta v(k+1) - \Delta v(k) \leq -v^{\min} + v(k-1)
\end{aligned}$$

In matrix form becomes:

$$\begin{bmatrix} 1 & 1 \\ -1 & -1 \end{bmatrix} \begin{bmatrix} \Delta v(k) \\ \Delta v(k+1) \end{bmatrix} \leq \begin{bmatrix} v^{\max} - v(k-1) \\ -v^{\min} + v(k-1) \end{bmatrix}$$

This will continue up to the control horizon $H_c$, then the general form for control variable constraint is expressed as:

$$\begin{bmatrix} 1 & 0 & 0 & \dots & 0 \\ 1 & 1 & 0 & \dots & 0 \\ \vdots & \vdots & \vdots & \ddots & \vdots \\ 1 & 1 & 1 & \dots & 1 \\ -1 & 0 & 0 & \dots & 0 \\ -1 & -1 & 0 & \dots & 0 \\ \vdots & \vdots & \vdots & \ddots & \vdots \\ -1 & -1 & -1 & \dots & -1 \end{bmatrix}_{2*H_c \times H_c} \begin{bmatrix} \Delta v(k) \\ \Delta v(k+1) \\ \\ \Delta v(k+H_c-1) \end{bmatrix} \le \begin{bmatrix} v^{\max} - v(k-1) \\ \vdots \\ v^{\max} - v(k-1) \\ -v^{\min} + v(k-1) \\ \vdots \\ -v^{\min} + v(k-1) \end{bmatrix}_{2*H_c \times 1} \tag{4.23}$$

### 4.4.2. Constraint on the Optimal Solution

Since the optimal solution $\Delta V$ is the vector contains the rate of change of the control signal which increments with length of control horizon.

The inequality constraint for the optimal solution can formulate as:

$$\Delta V^{\min} \le \Delta V \le \Delta V^{\max} \tag{4.24}$$

The constraint can express in two inequalities:

$$\Delta V \le \Delta V^{\max} \tag{4.25}$$

$$-\Delta V \le -\Delta V^{\min} \tag{4.26}$$

In matrix form becomes:

$$\begin{bmatrix} 1 \\ -1 \end{bmatrix} \Delta V \le \begin{bmatrix} \Delta V^{\max} \\ -\Delta V^{\min} \end{bmatrix}$$

$$\begin{bmatrix} 1 & 0 & \dots & 0 \\ 0 & 1 & \dots & 0 \\ \vdots & \vdots & \ddots & \vdots \\ 0 & 0 & \dots & 1 \\ -1 & 0 & \dots & 0 \\ 0 & -1 & \dots & 0 \\ \vdots & \vdots & \ddots & \vdots \\ 0 & 0 & \dots & -1 \end{bmatrix}_{2*H_c \times H_c} \begin{bmatrix} \Delta v(k) \\ \Delta v(k+1) \\ \vdots \\ \Delta v(k+H_c-1) \end{bmatrix} \le \begin{bmatrix} \Delta V^{\max} \\ \vdots \\ \Delta V^{\max} \\ -\Delta V^{\min} \\ \vdots \\ -\Delta V^{\min} \end{bmatrix}_{2*H_c \times 1} \tag{4.27}$$

### 4.4.3. Constraint on the Output Variable

Since the speed of the motor is the output of the plant, the following inequality constraint can express to satisfy the operation range of the incremental output variable.

$$y^{\min} \le y(k) \le y^{\max} \tag{4.28}$$

The constraint can be expressed in two inequalities:

$$y(k) \le y^{\max} \tag{4.29}$$

$$-y(k) \le -y^{\min} \tag{4.30}$$

At *k+1*moment and by substituting Equation (4.14) into (4.29) and (4.30), the constraint becomes:

$$\begin{aligned}
&y(k+1) \le y^{\max} \\
&\tilde{C}\tilde{A}X(k) + \tilde{C}\tilde{B}\Delta v(k) \le y^{\max} \\
&\tilde{C}\tilde{B}\Delta v(k) \le y^{\max} - \tilde{C}\tilde{A}X(k)
\end{aligned}$$

$$\begin{aligned}
&-y(k+1) \le -y^{\min} \\
&-\tilde{C}\tilde{A}X(k) - \tilde{C}\tilde{B}\Delta v(k) \le y^{\min} \\
&-\tilde{C}\tilde{B}\Delta v(k) \le -y^{\min} + \tilde{C}\tilde{A}X(k)
\end{aligned}$$

At *k+2* moment:

$$\begin{aligned}
&y(k+2) \le y^{\max} \\
&\tilde{C}\tilde{A}^2 X(k) + \tilde{C}\tilde{A}\tilde{B}\Delta v(k) + \tilde{C}\tilde{B}\Delta v(k+1) \le y^{\max} \\
&\tilde{C}\tilde{A}\tilde{B}\Delta v(k) + \tilde{C}\tilde{B}\Delta v(k+1) \le y^{\max} + \tilde{C}\tilde{A}^2 X(k)
\end{aligned}$$

$$\begin{aligned}
&-y(k+2) \le -y^{\min} \\
&-\tilde{C}\tilde{A}^2 x(k) - \tilde{C}\tilde{A}\tilde{B}\Delta v(k) - \tilde{C}\tilde{B}\Delta v(k+1) \le y^{\min} \\
&-\tilde{C}\tilde{A}\tilde{B}\Delta v(k) - \tilde{C}\tilde{B}\Delta v(k+1) \le -y^{\min} + \tilde{C}\tilde{A}^2 x(k)
\end{aligned}$$

The general form for the output constraint is:

$$
\begin{bmatrix}
\tilde{C}\tilde{B} & 0 & \dots & 0 \\
\tilde{C}\tilde{A}\tilde{B} & \tilde{C}\tilde{B} & \dots & 0 \\
\vdots & \vdots & \ddots & \vdots \\
\tilde{C}\tilde{A}^{H_p-1}\tilde{B} & \tilde{C}\tilde{A}^{H_p-2}\tilde{B} & \dots & \tilde{C}\tilde{A}^{H_p-H_c}\tilde{B} \\
-\tilde{C}\tilde{B} & 0 & \dots & 0 \\
-\tilde{C}\tilde{A}\tilde{B} & -\tilde{C}\tilde{B} & \dots & 0 \\
\vdots & \vdots & \ddots & \vdots \\
-\tilde{C}\tilde{A}^{H_p-1}\tilde{B} & -\tilde{C}\tilde{A}^{H_p-2}\tilde{B} & \dots & -\tilde{C}\tilde{A}^{H_p-H_c}\tilde{B}
\end{bmatrix}
\begin{bmatrix}
\Delta v(k) \\ \Delta v(k+1) \\ \vdots \\ \Delta v(k+H_c-1)
\end{bmatrix}
\le
\begin{bmatrix}
y^{\max} - \tilde{C}\tilde{A}x(k) \\ \vdots \\ y^{\max} - \tilde{C}\tilde{A}^{H_p}x(k) \\ -y^{\min} + \tilde{C}\tilde{A}x(k) \\ \vdots \\ -y^{\min} + \tilde{C}\tilde{A}^{H_p}x(k)
\end{bmatrix}
\tag{4.31}
$$

As defined Q and $\Delta V$ matrix in equation (4.15) then, equation (4.31) becomes:

$$
\begin{bmatrix} Q \\ -Q \end{bmatrix} \Delta V \le
\begin{bmatrix}
y^{\max} - \tilde{C}\tilde{A}x(k) \\ \vdots \\ y^{\max} - \tilde{C}\tilde{A}^{H_p}x(k) \\ -y^{\min} + \tilde{C}\tilde{A}x(k) \\ \vdots \\ -y^{\min} + \tilde{C}\tilde{A}^{H_p}x(k)
\end{bmatrix}
\tag{4.32}
$$

Finally, the MPC in the presence of constraints is proposed to find the optimal solution in the parameter vector $\Delta V$ that minimizes the cost function Equation (4.18) with subject to:

$$
\begin{bmatrix} Z_1 \\ Z_2 \\ Z_3 \end{bmatrix} \Delta V \le \begin{bmatrix} \sigma_1 \\ \sigma_2 \\ \sigma_3 \end{bmatrix}
\tag{4.33}
$$

Where the data matrices are:

$$
Z_1 = \begin{bmatrix}
1 & 0 & 0 & \dots & 0 \\
1 & 1 & 0 & \dots & 0 \\
\vdots & \vdots & \vdots & \ddots & \vdots \\
1 & 1 & 1 & \dots & 1 \\
-1 & 0 & 0 & \dots & 0 \\
-1 & -1 & 0 & \dots & 0 \\
\vdots & \vdots & \vdots & \ddots & \vdots \\
-1 & -1 & -1 & \dots & -1
\end{bmatrix}
\qquad
\sigma_1 = \begin{bmatrix}
v^{\max} - v(k-1) \\ \vdots \\ v^{\max} - v(k-1) \\ -v^{\min} + v(k-1) \\ \vdots \\ -v^{\min} + v(k-1)
\end{bmatrix},
$$

$$Z_2 = \begin{bmatrix} 1 & 0 & \dots & 0 \\ 0 & 1 & \dots & 0 \\ \vdots & \vdots & \ddots & \vdots \\ 0 & 0 & \dots & 1 \\ -1 & 0 & \dots & 0 \\ 0 & -1 & \dots & 0 \\ \vdots & \vdots & \ddots & \vdots \\ 0 & 0 & \dots & -1 \end{bmatrix} \qquad \sigma_2 = \begin{bmatrix} \Delta V^{\max} \\ \vdots \\ \Delta V^{\max} \\ -\Delta V^{\min} \\ \vdots \\ -\Delta V^{\min} \end{bmatrix}$$

$$Z_3 = \begin{bmatrix} Q \\ -Q \end{bmatrix} \qquad \sigma_3 = \begin{bmatrix} y^{\max} - \tilde{C}\tilde{A}x(k) \\ \vdots \\ y^{\max} - \tilde{C}\tilde{A}^{H_p}x(k) \\ -y^{\min} + \tilde{C}\tilde{A}x(k) \\ \vdots \\ -y^{\min} + \tilde{C}\tilde{A}^{H_p}x(k) \end{bmatrix}$$

Given that $J$ is a quadratic cost function and that the constraints are linear inequalities. For compactness of expression Equation (4.33) denoted as:

$$Z\Delta V \leq \sigma \tag{4.34}$$

Where $Z = \begin{bmatrix} Z_1 \\ Z_2 \\ Z_3 \end{bmatrix}$, and $\sigma = \begin{bmatrix} \sigma_1 \\ \sigma_2 \\ \sigma_3 \end{bmatrix}$

**Theorem 1-** Hamiltonian of optimal control theory

Consider

$$x_{k+1} = f(x_k, u_k) \tag{4.35}$$

$$J = \sum L(x_k, u_k) \tag{4.36}$$

The solution methods involve defining an additional function known as the control Hamiltonian

$$H(x_k, u_k) = L(x_k, u_k) + \lambda_k^T f(x_k, u_k) \tag{4.37}$$

The Lagrange multiplier $\lambda$ referred to as costate variable. The goal is to find an optimal control law $u^*$.

Using Theorem-1, to minimize the cost function $J$ subject to equality constraints by considering Lagrange multiplier λ, the Hamiltonian formulation is expressed as:

$$H = J + \lambda^T (Z\Delta V - \sigma) \tag{4.38}$$

By taking the first derivative on the Hamiltonian equation with respect to the vector $X(k)$ and $\lambda$ for minimization purpose.

The necessary conditions are:

$$\begin{aligned} \frac{\partial H}{\partial X} &= 0 \\ \frac{\partial H}{\partial \lambda} &= 0 \end{aligned} \tag{4.39}$$

Then,

$$\begin{aligned} &(\bar{Q}^T Q\bar{Q} + R)\Delta V + \bar{Q}^T Q(EX(k) - S_r) + Z^T \lambda = 0 \\ &\Delta V = -(\bar{Q}^T Q\bar{Q} + R)^{-1} \bar{Q}^T Q(EX(k) - S_r) - (\bar{Q}^T Q\bar{Q} + R)^{-1} Z^T \lambda \end{aligned} \tag{4.40}$$

$$\begin{aligned} &Z\Delta V - \sigma = 0 \\ &\Delta V = Z^{-1}\sigma \end{aligned} \tag{4.41}$$

Substituting Equation (3.73) in to (3.72):

$$\begin{aligned} &Z^{-1}\sigma = -(\bar{Q}^T Q\bar{Q} + R)^{-1} \bar{Q}^T Q(EX(k) - S_r) - (\bar{Q}^T Q\bar{Q} + R)^{-1} Z^T \lambda \\ &\lambda = -(Z(\bar{Q}^T Q\bar{Q} + R)^{-1} Z^T)^{-1} (\sigma + (\bar{Q}^T Q\bar{Q} + R)^{-1} Z^T \bar{Q}^T Q(EX(k) - S_r)) \end{aligned} \tag{4.42}$$

The first element from the optimal solution vector can be determined and used the control signal to the system. Since $v$ is assigned for quadrature current $I_q$ and obtained as:

$$v(k) = \Delta v + v(k-1)$$

Therefore, by substituting Equation (4.37) into plant (4.15) to obtain the predicted state variable and output variable. And continued the prediction process by taking the updated optimal solution. The control signal from the outer loop is a reference to the next inner loop current control ($I_q$).

# CHAPTER FIVE

# 5. SIMULATION RESULT AND DISCUSSION

In this chapter, the proposed approach is applied to a PMSM in the case of Hyundai ATOS vehicle to illustrate effectiveness and applicability. The dynamic model of the PMSM has been introduced in chapter three and the parameters used in simulation are listed in Table 3-3.

## 5.1. Simulation Result of a PMSM without Vehicle Load

The proposed approach to control the speed of the motor is used MPC and in chapter three, MPC is clearly developed and designed. In this section the system performance of MPC, LQR, and GA based PI controllers are discussed and compared for a PMSM. The outer loop of the system is selectively controlled by the listed approaches while the inner loop regulated by PI controller for all approaches. The constraint on the input and output variable of the plant to design MPC are considered as follows:

$$
\begin{aligned}
-40 &\le v(k) \le 40 \\
-350 &\le x(k) \le 350
\end{aligned}
$$

$H_p = 5$ and $H_c = 4$ are used for prediction control. And the weighting matrix for the cost function is obtained through GA tuning technique for both MPC and LQR approaches.

$$
\begin{aligned}
\bar{Q} &= 152.5 \\
R &= 70.6
\end{aligned}
$$

For PI speed control and current control, the gain parameters are obtained by GA tuning algorithm.

*Table 5-1: Optimal gain value OF GA-PI*

| Gain | Speed | Id | Iq |
|---|---|---|---|
| **Kp** | 0.8 | 1 | 5.3 |
| **Ki** | 227.4 | 156.2 | 172.02 |

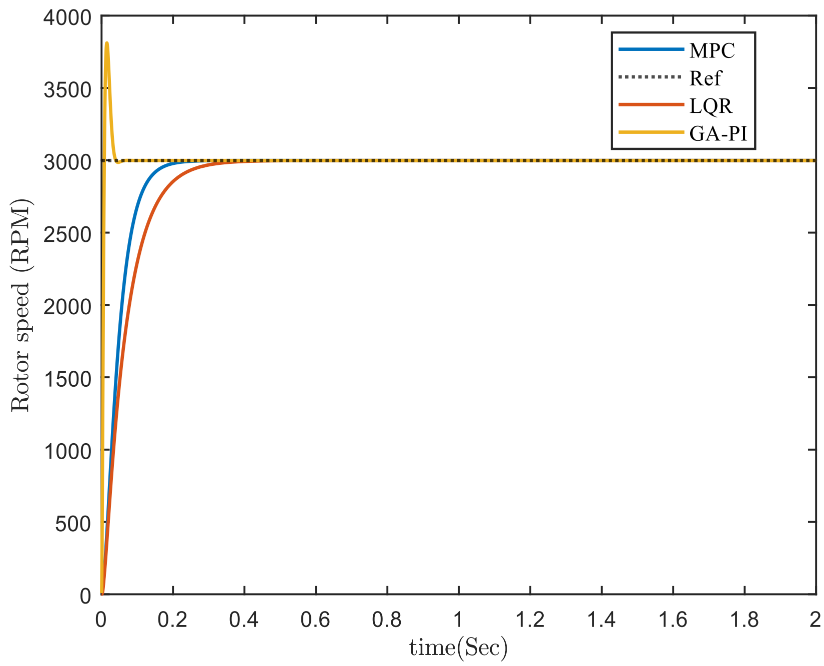


*Figure 5-1: Rotor speed and desired speed using MPC, LQR and GA-PI without vehicle load*

From figure 5-1, recorded the response performance in Table 5-3 as settling time, rise time and overshoot of the response without torque load then the proposed MPC is better performed than LQR and GA-PI for the given reference speed 3000 RPM as compared each other.

Figure 5-2, expressed the control signal of the outer loop speed response and compared with the two different controllers. As considering a constraint on the control input for the MPC from the given rated current of the motor the proposed MPC controller taken an action within the range quickly, at the same time the control signal of LQR and PI are acted out of the range on the starting time.

*Table 5-2: System performance of MPC, LQR and GA-PI without vehicle load*

| | MPC | LQR | GA-PI |
|---|---|---|---|
| **Rising time(sec)** | 0.045 | 0.1097 | 0.014 |
| **Settling time (sec)** | 0.080 | 0.1993 | 0.034 |
| **Overshoot (%)** | 0 | 0 | 27.1 |

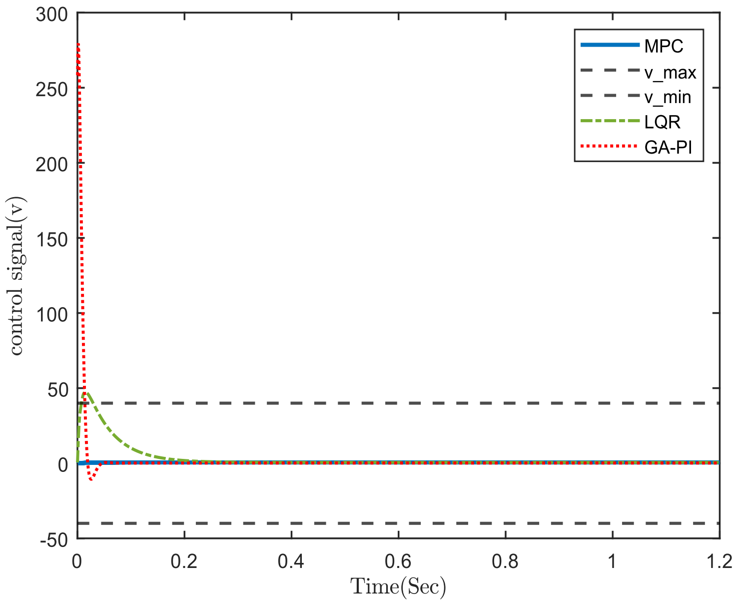


*Figure 5-2: Outer loop Control signal of MPC, LQR and GA-PI*

Figure 5-3 shows the error between the actual and desired speed of the PMSM and compared the proposed MPC, LQR and GA-PI controllers. Then the proposed MPC has less error than others controllers.

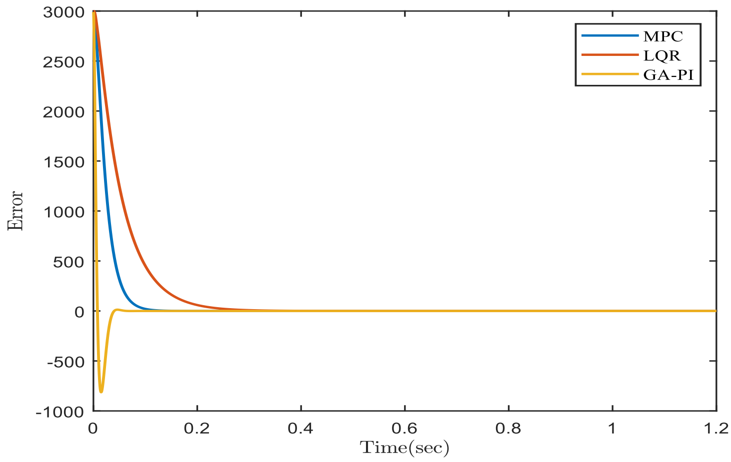


*Figure 5-3: Error between desired and actual speed of a PMSM without vehicle load*

The current response of the d-and q-axis are shown in the Figure 5-4. The d-axis current response followed the desired signal, and the q-axis current followed the reference signal from MPC controller as controlled by PI.

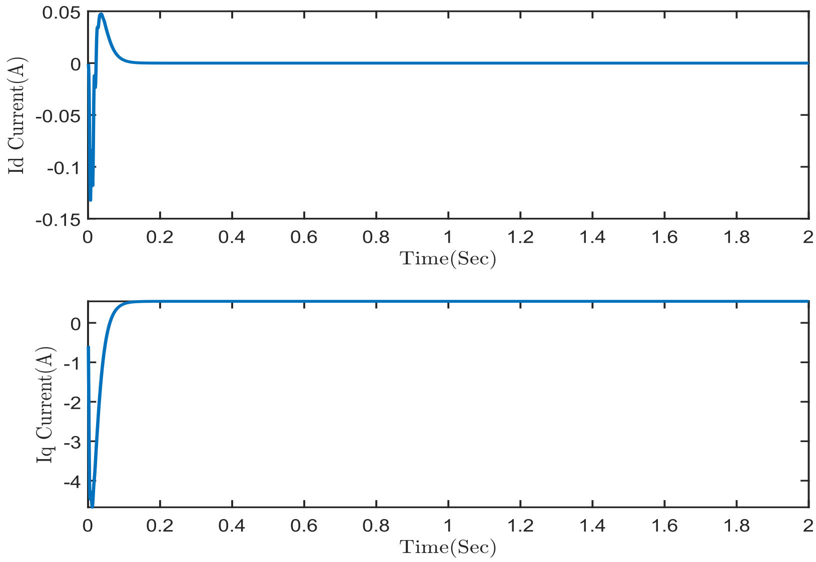


*Figure 5-4: d-q Current response without vehicle load*

Figure 5-5 shows, the control signal of the inner loop PI controller. This is called the voltage $V_{d\text{-}q}$, after applying the inverse clark-park transformation the signal utilized as a reference to SVPWM to generate a pulse signal.

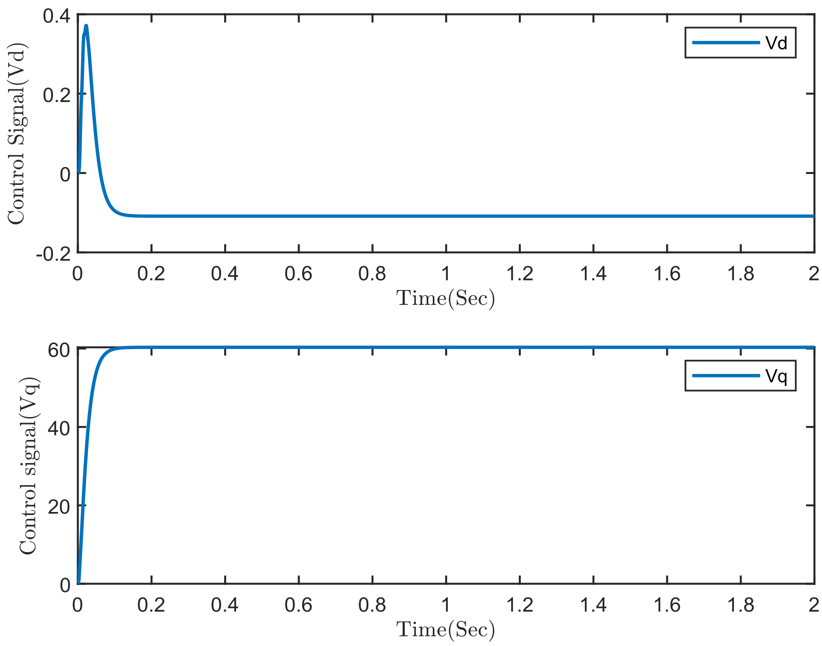


*Figure 5-5: Voltage Vd-q response*

### 5.2. Set Point Change of a PMSM with Vehicle Load

In chapter three, the total torque load required by Hyundai ATOS vehicle is calculated around 85Nm. So, the calculated torque was applied to the motor model in the simulation. The result still the proposed MPC is superiorly performed than LQR and GA-PI controllers. The comparison of speed response shown in Figure 5-6 describing that the speed response using MPC can reach at steady state faster than LQR and GA-PI controllers. At starting time, from the LQR controller response the motor acts as reverse rotation.

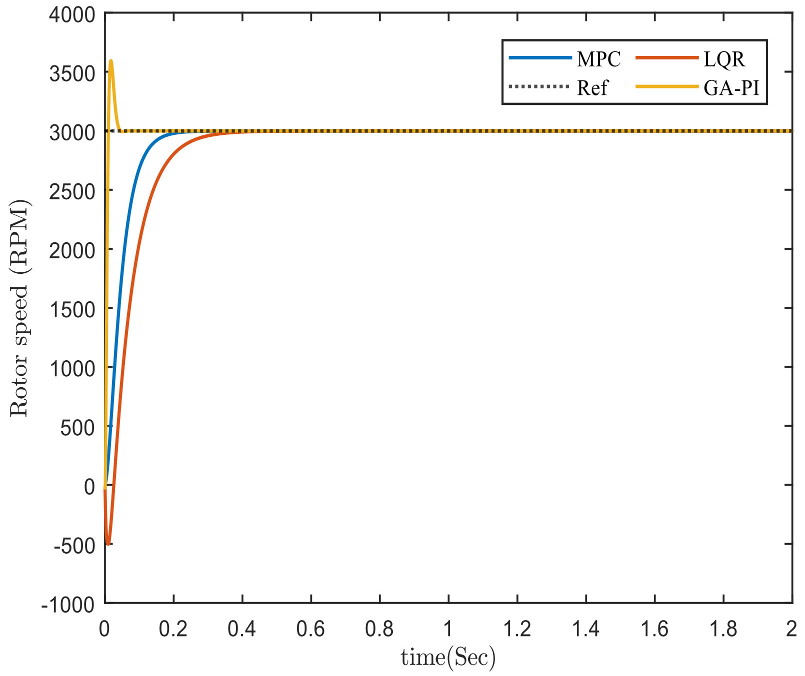


*Figure 5-6: Rotor speed and desired speed using MPC, LQR and GA-PI with vehicle load*

Table 5-4 illustrated the system performance of a PMSM using MPC, LQR and GA-PI controllers with vehicle load. The proposed MPC approach is effectively performed for the system with load torque without any overshoot and settled as fast as possible than other approach.

*Table 5-3: System performance of MPC, LQR and GA-PI with vehicle load*

| | MPC | LQR | GA-PI |
|---|---|---|---|
| **Rising time(sec)** | 0.0317 | 0.109 | 0.0066 |
| **Settling time (sec)** | 0.0623 | 0.2061 | 0.0367 |
| **Overshoot (%)** | 0 | 0 | 19.82 |

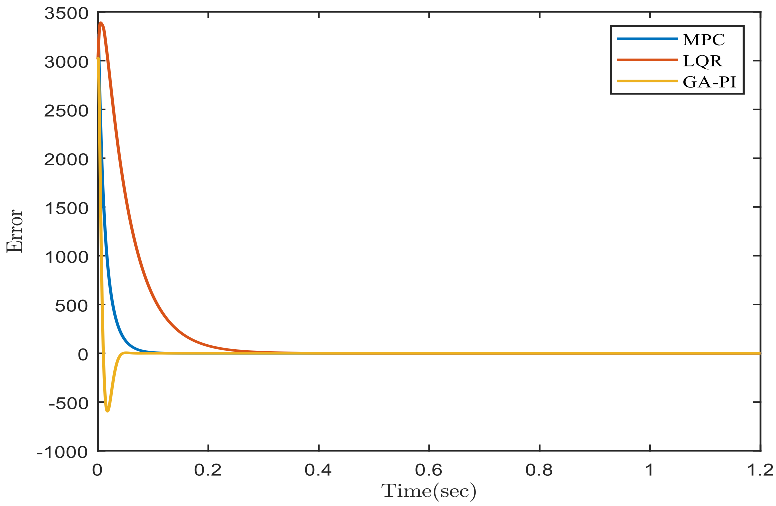


*Figure 5-7: Error between desired and actual speed of a PMSM with vehicle load*

Figure 5-7 illustrated the error difference between the targeted and the actual speed response of the PMSM using MPC, LQR and GA-PI controller. The proposed MPC approach is minimizes the error as fast as possible than LQR and GA-PI controllers.

The rated stator current of the PMSM is 120A and its value is the magnitude of d-q current. As controlled the current by PI, the response of Iq as shown in the Figure 5-8, about 90A gives to operate the motor at the desired speed fed with the proposed vehicle Hyundai ATOS.

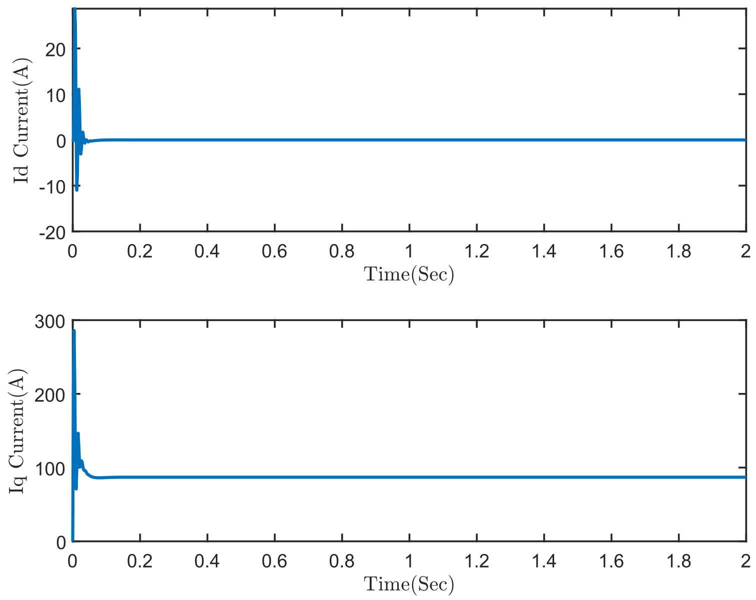


*Figure 5-8: d-q Current response with vehicle load*

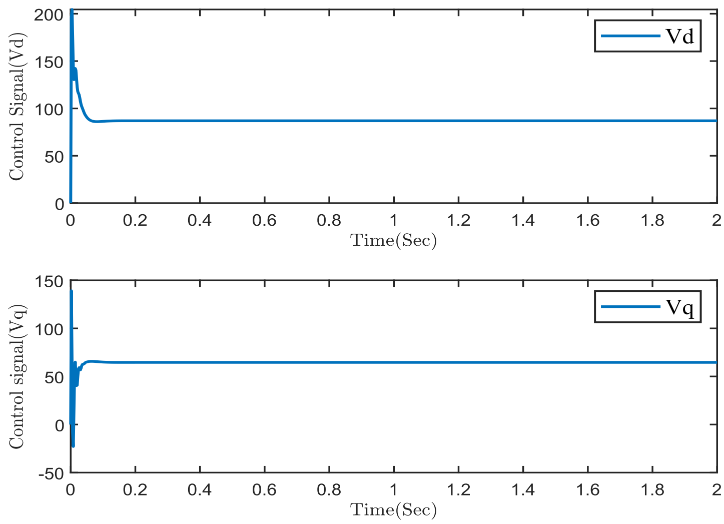


*Figure 5-9: Vdq voltage with vehicle load*

Figure 5-9 shown the response of the control signal of inner loop PI control as considering the torque load on the PMSM. These are an action signal as voltage Vd-q signal and they are a reference signal to SVPWM to generate the pulse signal for inverter.

### 5.3. Speed Changes on a PMSM with Vehicle Load

As discussed before, the rated speed of the motor is 314 rad/sec (or 3000 rpm) and the proposed MPC approach is effectively regulated the targeted speed of the motor with vehicle load. The Proposed MPC is also tested by two cases to show the speed variation of the motor.

**Case- 1:** From 1900 RPM (0 to 0.6 sec) then 2400 RPM (0.4-1.2 sec) and finally 3000 RPM (from 1.2 sec).

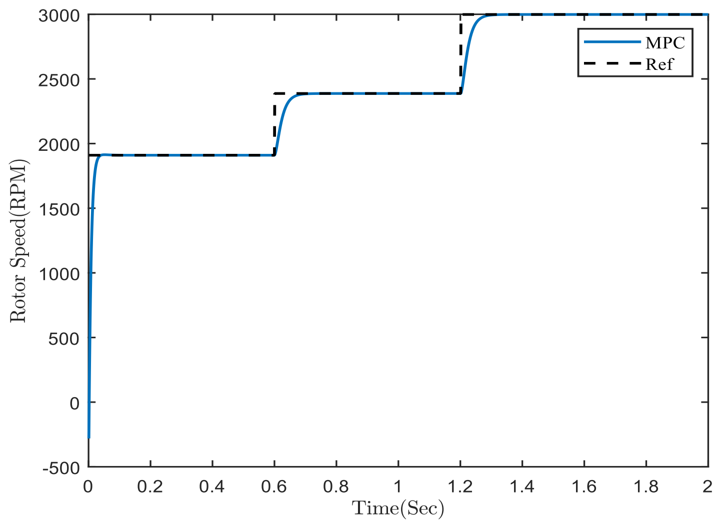


*Figure 5-10: Result of speed variation of a PMSM for case-1*

**Case-2:** From 1900 RPM (0 to 0.6 sec) then 3000 RPM (0.4-1.2 sec) and finally 1400 RPM (from 1.2 sec).

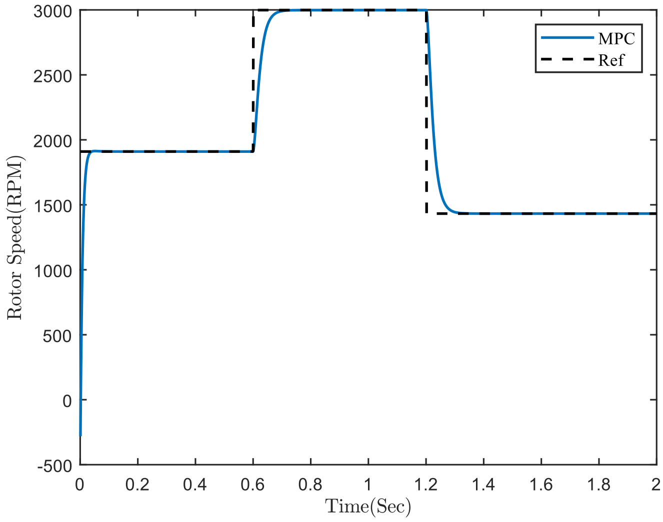


*Figure 5-11: Result of speed variation of a PMSM for case-2*

## 5.4. Disturbance Rejection Rerformance of the Controllers

The PMSM drive is proposed to propel the Hyundai ATOS vehicle. Many factors can happen to the vehicle while riding in the road. In this thesis, considered the forces imposed to the vehicle and analyzed the power to overcome them. The total torque load of the vehicle is 85 Nm, if a sudden change happens on the road condition like the slope of the uphill of the road or the mass variation of persons affect to load, assuming the torque load is increases up to 110 Nm.

**Uphill case:** Adding the disturbance 25 Nm in the torque load at the simulation time t=0.6 sec and out at t=1.2 sec as shown in Figure 5-12.

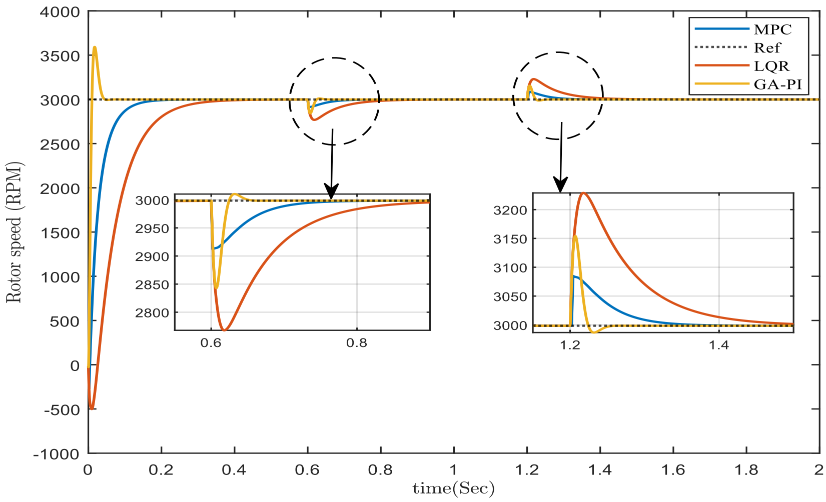


*Figure 5-12: Rotor speed with disturbance uphill case*

From the Figure 5-12 shown, when the disturbance is added at 0.6s the speed of the motor is decreased for all controllers but the proposed MPC is better performed than LQR and GA-PI. MPC came back to the desired speed with small undershoot and good settling time than others.

**Load variation case**: Adding the disturbance 15 Nm in the torque load from initial. In this case if any load change happens before the vehicle starting movement like payload change. By assuming 15 Nm added to the torque load and the result is shown in the Figure 5-13, MPC is better tracked the desired speed than other controllers.

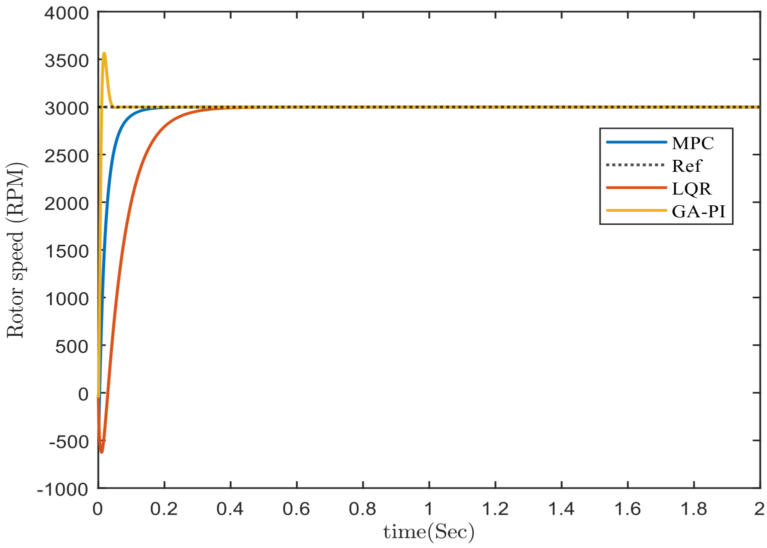


*Figure 5-13: Rotor speed with disturbance load variation case*

## 5.5. Electromagnetic Torque of a PMSM

Electromagnetic torque is analyzed to evaluate the performance of the PMSM. At starting time, the developed torque by the motor is high due to start safely with high starting current and settled on the required load torque. The simulation conducted on different operation conditions to determine the effectiveness of the motor. Figure 5-14 shown the torque developed by PMSM to propel the vehicle by 85 Nm.

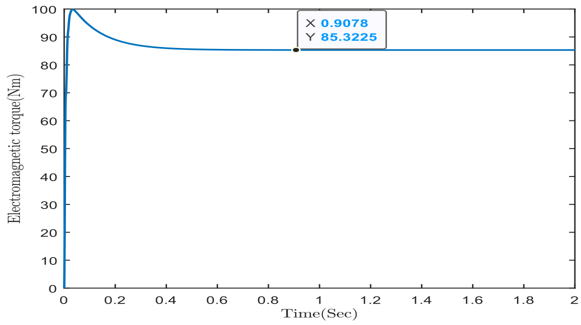


*Figure 5-14: Electromagnetic torque with vehicle load*

Figure 5-15 illustrated the uphill disturbance case, 25Nm is happened at t=0.6 sec and out at t=1.2 sec. Therefore, the required torque automatically developed 110Nm to tolerate the disturbance.

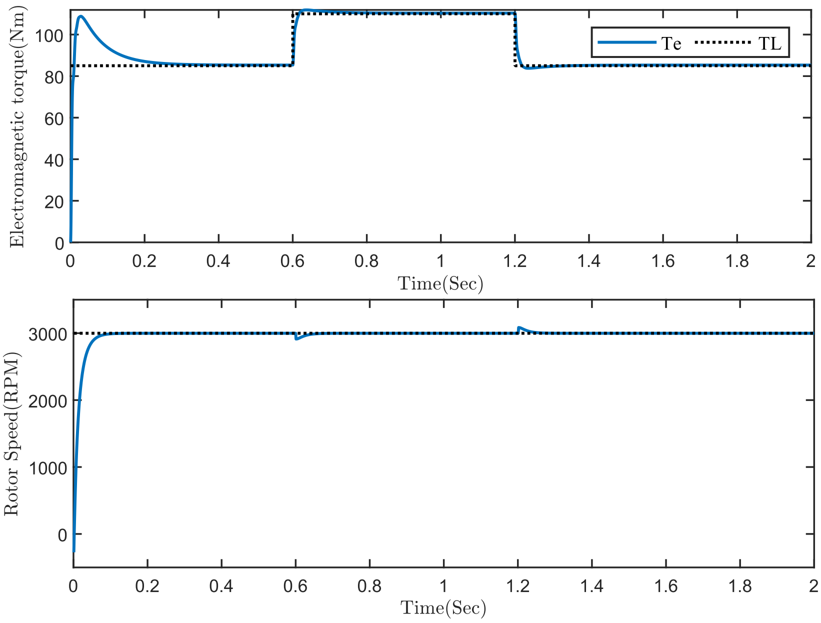


*Figure 5-15: Electromagnetic torque uphill disturbance case*

Figure 5-16 shown the torque, from the speed variation of the PMSM as described in Figure 5-11

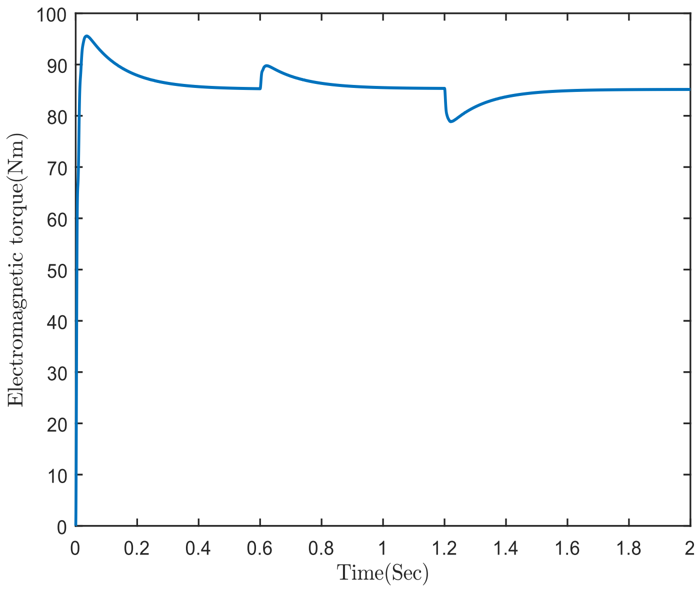


*Figure 5-16: Electromagnetic torque under speed variation*

### 5.6. Simulation Result of SVPWM and Inverter

SVPWM utilized for precise control of the inverter output voltage by generating three phase waveforms with specific magnitudes and angles. These waveforms are formed by switching the inverter power devices (IGBTs) at high frequencies. By adjusting the PWM duty cycle of the switching signal the desired voltage waveform is performed as shown in Figure 5-17.

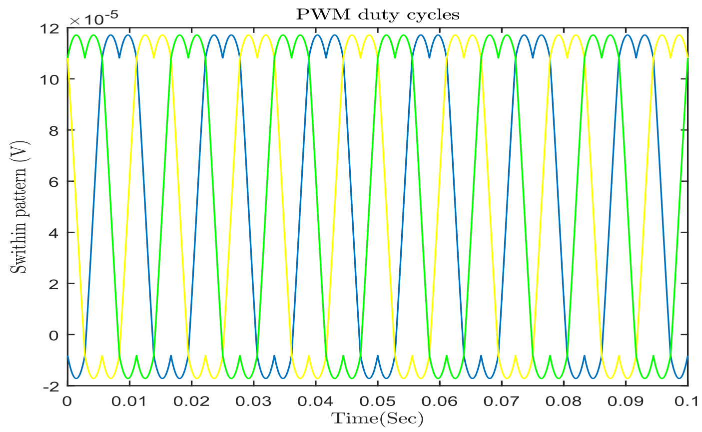


*Figure 5-17: PWM duty cycle*

The phase voltage that are generated from the inverter as shown in the Figure 5-18, have three steps 0, $\pm\frac{1}{3}$Vdc, $\pm\frac{2}{3}$Vdc derived from the pulse signal based on the SVPWM technique.

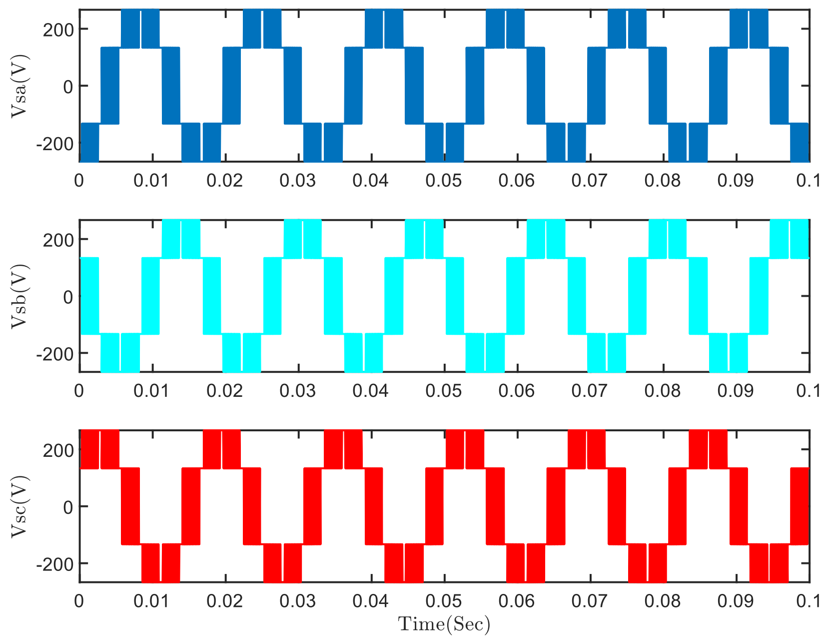


*Figure 5-18: Three phase voltage source from inverter*

# 6. CONCULSION AND RECOMMENDATION

## 6.1.Conclusion

This thesis focuses on the designing of model predictive speed control of a PMSM for the application of Hyundai ATOS vehicle. Based on the study of the dynamic model of PMSM drive system, the control strategy MPC is designed for the outer loop speed control and cascaded with the PI control strategy for inner loop current control.

The different forces imposed to the vehicle, the power required to overcome these forces and the required torque to propel the vehicle are analyzed based on the dynamic model of the vehicle using the parameters of the Hyundai ATOS car. According to this, the appropriate motor is selected based on the power requirement of the vehicle.

The proposed MPC is compared with LQR and GA-PI controller to assure the performance of the strategy. The PI gain value and weighting matrix for cost function for both MPC and LQR were tuned by GA method. Thus, the algorithm provided better result and they have also succeeded in providing a good response on speed and current control. From the simulation result, the proposed method obtained better performance and effective than LQR and GA-PI approaches. From the time response of the system, the proposed MPC has been performed 0.031 sec rising time, 0.062 sec settling time and 0% overshoot. The robustness of the proposed strategy is evaluated by a sudden disturbance on the torque load and then the response is tolerated the load disturbance with a short period of time. Moreover, the developed torque is also responsible to produce a rotational motion for the proposed vehicle.

## 6.2.Recommendation

In recent years, the demand of EVs are increased rapidly. This topic has a significant reputation due to the growing demand for efficient and precise control of electric motor drive in EVs. MPC is a powerful control technique that has gained considerable attention currently. Its ability to handle complex systems with multiple constraints makes it an ideal candidate for advanced control strategies in EV application. In this thesis, employing MPC for speed control of a PMSM in an EV, through this strategy can achieve to the enhancement of battery efficiency, optimization of energy consumption and improvement of the system performance. For experimental validation, by conducting practical implementation using a prototype EV or hardware in the loop setup to evaluate the performance of the MPC based speed control of a PMSM is highly recommended. Through the implementation can evaluate the controller capability to accomplish the accurate speed regulation, responding to dynamic load conditions and maintain stability under varying operating conditions.

Furthermore, it is highly recommended considering the implementation of torque control for PMSM as it has the potential to revolutionize motor control strategies and providing significant advantages for EVs.

## Acknowledgments

The research for this paper was financially supported by Adama Science and Technology University under the grant number of **ASTU/SM-R/727/23**, Adama, Ethiopia.

# REFERENCES

Aja Zarma, T., Adamu Galadima, A., & Aminu, M. A. (2019). *Review of Motors for Electrical Vehicles*. *1*. https://doi.org/10.9734/JSRR/2019/v24i630170

Akhtar, M. J., Behera, R. K., & Parida, S. K. (2016). Propulsion system design of electric vehicle. *2015 6th International Conference on Power Electronics Systems and Applications: Electric Transportation - Automotive, Vessel and Aircraft, PESA 2015*. https://doi.org/10.1109/PESA.2015.7398900

Atamnia, K., Lebaroud, A., & Makhlouf, M. (n.d.). TRACTION MOTOR SELECTION BASED ON THE PERFORMANCE ANALYSIS OF PURE ELECTRIC VEHICLE UNDER DIFFERENT DRIVING SCENARIOS. *Carpathian Journal of Electrical Engineering*, *14*(1), 2020.

Cao, W., … A. B.-… R. J. of, & 2019, undefined. (n.d.). Review of electrical motor drives for electric vehicle applications. *Search.Informit.Org*. https://doi.org/10.22581/muet1982.1903.01

Chai, S., Wang, L., & Rogers, E. (2013). Model predictive control of a permanent magnet synchronous motor with experimental validation. *Control Engineering Practice*, *21*(11), 1584–1593. https://doi.org/10.1016/J.CONENGPRAC.2013.07.008

Deng, J., Bae, C., Denlinger, A., & Miller, T. (2020). Electric Vehicles Batteries: Requirements and Challenges. *Joule*, *4*(3), 511–515. https://doi.org/10.1016/J.JOULE.2020.01.013

Gao, J., Zhang, J., Fan, M., Peng, Z., Chen, Q., & Zhang, H. (2021). *Model Predictive Control of Permanent Magnet Synchronous Motor Based on State Transition Constraint Method*. https://doi.org/10.1155/2021/3171417

Garcia, C., Rodriguez, J., Odhano, S., Zanchetta, P., & Davari, S. A. (2019). Modulated Model Predictive Speed Control for PMSM Drives. *2018 IEEE International Conference on Electrical Systems for Aircraft, Railway, Ship Propulsion and Road Vehicles and International Transportation Electrification Conference, ESARS-ITEC 2018*. https://doi.org/10.1109/ESARS-ITEC.2018.8607701

Guan, Y., Zhu, Z., Afinowi, I., … J. M.-… on E. M., & 2014, undefined. (n.d.). Difference in maximum torque-speed characteristics of induction machine between motor and generator operation modes for electric vehicle application. *Ieeexplore.Ieee.Org*.

Retrieved March 22, 2023, from https://ieeexplore.ieee.org/abstract/document/6960170/

Hasan, M. S., Sharaf, A. F., Albakhait, M. D., & Jaber, A. I. (2020). High Performance Rectifier/Multilevel Inverter Based BLDC Motor Drive with PI Controller. *IOP Conference Series: Materials Science and Engineering*, *745*(1). https://doi.org/10.1088/1757-899X/745/1/012005

Huang, G., Li, J., Yu, H., Huang, W., & Zhao, K. (2022). Generalized predictive speed control based on equivalent-input-disturbance for PMSM drive system. *Advances in Mechanical Engineering*, *14*(10). https://doi.org/10.1177/16878132221132154/ASSET/IMAGES/LARGE/10.1177_16878132221132154-FIG2.JPEG

Huang, X., Pan, H., & Yuan, K. (2020). Speed and Current Control of PMSM based on Double MPC. *Proceedings - 2020 7th International Forum on Electrical Engineering and Automation, IFEEA 2020*, 300–304. https://doi.org/10.1109/IFEEA51475.2020.00070

Huang, Y., Xu, Y., Zhang, W., & Zou, J. (2020). Modified Single-Edge SVPWM Technique to Reduce the Switching Losses and Increase PWM Harmonics Frequency for Three-Phase VSIs. *IEEE Transactions on Power Electronics*, *35*(10), 10643–10653. https://doi.org/10.1109/TPEL.2020.2975626

in, A. Y.-I. J. of E. T., & 2015, undefined. (n.d.). Space vector pulse width modulation technique. *Researchgate.Net*. Retrieved May 4, 2023, from https://www.researchgate.net/profile/Ayman-Yousef-6/publication/282859193_Space_Vector_Pulse_Width_Modulation_Technique/links/574db33a08ae8bc5d15bf37b/Space-Vector-Pulse-Width-Modulation-Technique.pdf

Krishnan, R. (1991). Application Characteristics of Permanent Magnet Synchronous and Brushless dc Motors for Servo Drives. *IEEE Transactions on Industry Applications*, *27*(5), 986–996. https://doi.org/10.1109/28.90357

Kumar, H., Dhanvijay, Maneetkumar. R., Maravulla, R., & Patil, Sudhir. M. (2022). An Overview of Efficiency Improvement Strategies for Electric Vehicle Drivetrain using PMSM Drives to mitigate EV Range Anxiety. *2022 International Conference on*

*Innovations in Science and Technology for Sustainable Development (ICISTSD)*, 24–29. https://doi.org/10.1109/ICISTSD55159.2022.10010387

Magazine, T. J.-I. E., & 2017, undefined. (n.d.). Getting rare-earth magnets out of EV traction machines: A review of the many approaches being pursued to minimize or eliminate rare-earth magnets from future EV. *Ieeexplore.Ieee.Org*. Retrieved March 22, 2023, from https://ieeexplore.ieee.org/abstract/document/7873383/

Mao, H., Tang, X., & Tang, H. (2022). Speed control of PMSM based on neural network model predictive control. *Transactions of the Institute of Measurement and Control*, *44*(14), 2781–2794. https://doi.org/10.1177/01423312221086267

Minyamer Gelawe, G. (2020). *Artificial Intelligence Based Non-linear PID Speed and Current Control of Brushless DC Motor for Electric Vehicle Drive. (The Case of Bajaj Qute)*. http://213.55.101.20:8080/xmlui/handle/123456789/1506

Murali, A., Wahab, R., Gade, C., … C. A.-W. E. V., & 2021, undefined. (n.d.). Assessing finite control set model predictive speed controlled PMSM performance for deployment in electric vehicles. *Mdpi.Com*. Retrieved May 24, 2023, from https://www.mdpi.com/1030562

Muthukumar, M., Rengarajan, N., Velliyangiri, B., Omprakas, M. A., Rohit, C. B., & Raja, U. K. (2021). The development of fuel cell electric vehicles – A review. *Materials Today: Proceedings*, *45*, 1181–1187. https://doi.org/10.1016/J.MATPR.2020.03.679

Oubelaid, A., Taib, N., Nikolovski, S., Alharbi, T. E. A., Rekioua, T., Flah, A., & Ghoneim, S. S. M. (2022). Intelligent Speed Control and Performance Investigation of a Vector Controlled Electric Vehicle Considering Driving Cycles. *Electronics 2022, Vol. 11, Page 1925*, *11*(13), 1925. https://doi.org/10.3390/ELECTRONICS11131925

Rauth, S. S., & Samanta, B. (2020). Comparative Analysis of IM/BLDC/PMSM Drives for Electric Vehicle Traction Applications Using ANN-Based FOC. *2020 IEEE 17th India Council International Conference, INDICON 2020*. https://doi.org/10.1109/INDICON49873.2020.9342237

Ren, W., Wu, Y., Conference, R. D.-2020 39th C. C., & 2020, undefined. (n.d.). A vector control system of PMSM with the assistance of fuzzy PID controller. *Ieeexplore.Ieee.Org*. Retrieved April 19, 2023, from https://ieeexplore.ieee.org/abstract/document/9189325/

S Chauhan - International journal of scientific & technology, & 2015, undefined. (n.d.). Motor torque calculations for electric vehicle. *Academia.Edu*. Retrieved June 20, 2023, from https://www.academia.edu/download/60814999/Motor_Torque_Calculations_For_Electric_Vehicle20191006-126594-1gwy5v2.pdf

Sudjoko, R. I., Hartono, & Iswahyudi, P. (2020). Speed Control of Permanent Magnet Synchronous Motor Using Universal Bridge and PID Controller. *Lecture Notes in Mechanical Engineering*, 405–416. https://doi.org/10.1007/978-981-15-4481-1_39/COVER

Tan, K., Su, J., … H. W.-2020 T. 46th A. C. of, & 2020, undefined. (n.d.). MPC Based Full-speed Domain Control Strategy of Interior Permanent Magnet Synchronous Motor. *Ieeexplore.Ieee.Org*. Retrieved April 19, 2023, from https://ieeexplore.ieee.org/abstract/document/9255410/

Tian, M., Cai, H., Zhao, W., Energies, J. R.-, & 2023, undefined. (n.d.). Nonlinear Predictive Control of Interior Permanent Magnet Synchronous Machine with Extra Current Constraint. *Mdpi.Com*. Retrieved April 19, 2023, from https://www.mdpi.com/2056712

Varga, B. O., Sagoian, A., & Mariasiu, F. (2019). Prediction of Electric Vehicle Range: A Comprehensive Review of Current Issues and Challenges. *Energies 2019, Vol. 12, Page 946*, *12*(5), 946. https://doi.org/10.3390/EN12050946

Vempalli, S. K., Ramprabhakar, J., Shankar, S., & Prabhakar, G. (2018). Electric Vehicle Designing, Modelling and Simulation. *2018 4th International Conference for Convergence in Technology, I2CT 2018*. https://doi.org/10.1109/I2CT42659.2018.9058161

Workineh, T. G., Yetayew, T. T., & Egziabher, A. G. (2021). Modeling and Analysis of Three-Phase Inverter for Induction Motor Drive for Three-Wheel Electric Vehicle Application. *Lecture Notes of the Institute for Computer Sciences, Social-Informatics and Telecommunications Engineering, LNICST*, *384*, 170–183. https://doi.org/10.1007/978-3-030-80621-7_13

Yang, Y., He, Q., Fu, C., Liao, S., & Tan, P. (2020). Efficiency improvement of permanent magnet synchronous motor for electric vehicles. *Energy*, *213*, 118859. https://doi.org/10.1016/J.ENERGY.2020.118859

Younesi, A., Tohidi, S., Feyzi, M. R., & Baradarannia, M. (2018). An improved nonlinear model predictive direct speed control of permanent magnet synchronous motors. *International Transactions on Electrical Energy Systems*, *28*(5). https://doi.org/10.1002/ETEP.2535

Zhu, X., Quan, L., Chen, Y., Liu, G., Shen, Y., & Liu, H. (2012). Permanent magnet online magnetization performance analysis of a flux mnemonic double salient motor using an improved hysteresis model. *Journal of Applied Physics*, *111*(7). https://doi.org/10.1063/1.3676049

**Reference link:**

[L1] - https://www.caranddriver.com/features/g43480930/history-of-electric-cars/

[L2] - Darkening Day: Air Pollution Films and Environmental Awareness, 1960–1972 – Medicine on Screen (nih.gov)

[L3] - https://electronics.stackexchange.com/questions/302170/spikes-dc-motor-current sensing

[L4] - https://electricalacademia.com/induction-motor/three-phase-induction-motor-construction/

[L5] - https://www.electrical4u.net/induction-motor/switched-reluctance-motor-srm-construction-working-types-advantages/

[L6] - https://www.researchgate.net/figure/Block-Diagram-of-LQR Controller_fig2_332577566

The History of the Electric Vehicle (historycooperative.org)

[L7] - https://cdn.hyundai.co.za/Documents/Atos_Specifications.pdf

# APPENDICES

## Appendix A : Matlab code for analysis motive forces with approaching angle of the vehicle.

```
m=1310; g=9.81; a=0.5;
r=0.2; kr=0.01; kad=0.33;
eff=0.98; nd=1.23; af=2.18;
f_tot=0; vkph=100; ang=0;
ang1=20; d_ang=1e-2; ang_final=ang1;
x=1; n=1;
while (ang<ang_final);
vmps=vkph*(1000/3600);
theta=ang *(2*pi/360);
Fa=0.5*nd*kad*af*(vmps)^2;
if ang<=100*d_ang
statfic=0.001;
else
statfic=0;
end
Frolling=m*g*(kr+statfic)*cos(theta);
Fgradient=m*g*sin(theta);
F_tot=Frolling+Fgradient+Fa;
ang=ang+d_ang;
if x >16
F_totn(n)=F_tot;
Frollingn(n)=Frolling;
Fgradientn(n)=Fgradient;
F_an(n)=Fa;
angn(n)=ang;
n=n+1;
x=1;
end
x=x+1;
end
figure(1);
plot(angn,F_totn,'k',angn,Fgradientn,'r',
angn,Frollingn,'k:',angn,F_an,'b--','linewidth',1.5)
axis([0 20 0 4500]);
legend('Total force','Gradient Force','Rolling Force','Aerodynamic
Force')
grid
title('Motive Force verses Approching Angle','Interpreter','Latex')
xlabel('Approaching Angle','Interpreter','Latex')
ylabel('Motive Force(N)','Interpreter','Latex')
```

## Appendix B: Matlab code for analysis desire power and speed of the vehicle

```
m=1310; g=9.81; a=0.5;
r=0.2; kr=0.01; kad=0.33;
eff=0.98; nd=1.23; af=2.18;
f_tot=0; vkph=0; vkph1=0; ang=0;
ang1=20; d_vkph=1e-2; vkph_final=100;
x=1; n=1;
while (vkph<vkph_final);
vmps=vkph*(1000/3600);
theta=ang *(2*pi/360);
Fa=0.5*nd*kad*af*(vmps)^2;
```

```
if vkph<=100*d_vkph
statfric=0;
else
statfric=0;
end
Frolling=m*g*(kr+statfric)*cos(theta);
Fgradient=m*g*sin(theta);
F_tot=Frolling+Fa+Fgradient+m*a;
power=F_tot*vmps/0.95;
vkph=vkph+d_vkph;
vkph1=vkph1+d_vkph;
if x >16
powern(n)=power/1000;
vkphn(n)=vkph;
n=n+1;
x=1;
end
x=x+1;
end
figure(1);
plot(vkphn,powern,'k','linewidth',1.5)
axis([0 100 0 40]);
%legend('Total force','Gradient Force','Rolling Force','Aerodynamic
Force')
% grid
title('Power verses Speed of Car in km/hr','Interpreter','Latex')
xlabel('Speed of the car(km/hr)','Interpreter','Latex')
ylabel('power(kW)','Interpreter','Latex')
```

## Appendix C: Matlab code for MPC controller with motor dynamics

```
global p pm J bbb Tl dd

pm=0.192; p=4; bbb=0.002; J=0.011; Tl=0;
dd=Tl*p/J;
Ac=-bbb/J; Bc=(3*p)*pm/(2*J); Cc=1;
Dc=0;
Delta_t=0.02;
[Ad,Bd,Cd,Dd]=c2dm(Ac,Bc,Cc,Dc,Delta_t); % discteretization
[m1,n1]=size(Cd);
[n1,n_in]=size(Bd);
%agumentaion
A=eye(n1+m1,n1+m1);
A(1:n1,1:n1)=Ad;
A(n1+1:n1+m1,1:n1)=Cd*Ad;
B=zeros(n1+m1,n_in);
B(1:n1,:)=Bd;
B(n1+1:n1+m1,:)=Cd*Bd;
C=zeros(m1,n1+m1);
C(:,n1+1:n1+m1)=eye(m1,m1);
D=Dd;
Hp=5; Hc=4;
Q=152.5*C*C';
R=70.6*eye(Hc);

v_max=40; v_min=-v_max;
deltav_max=0.5; deltav_min=-deltav_max;
y_max=350; y_min=y_max;
[F, phi] = F_phi(A, B, C, Hp, Hc);
```

```
E=phi'*Q*phi+R;
M1=[eye(Hc);-eye(Hc)];
M2=zeros(Hc);
for j=1:Hc
    for i=1:Hc
        if i<=j
            M2(j,i)=1;
        end
    end
end
M2=[M2;-M2];
M3=[phi;-phi];
M=[M1;M2;M3];
gamma1=[deltav_max*ones(Hc,1);-deltav_min*ones(Hc,1)];

Sref=314*ones(Hp,1);
Idref=0;

kp1=0.2707; ki1=266.9787;
kp2=0.3394; ki2=371.9215;

x=[0 0 0]'; t=0; h=0.001; loop=1000;
buf2=[]; buf3=[]; buf4=[];
buf=[]; us=0; xm=0; xm_old=xm; ym=0;
xf=[xm-xm_old;ym];
z1=0; z2=0; ee1=0; ee2=0;
for i=1:loop
    Vg_rms= 380/sqrt(2);
wg = 2*pi*60;
Vga=Vg_rms*sin(wg*t - pi/2);            %grid voltage A phase%
Vgb=Vg_rms*sin(wg*t- 2*pi/3 - pi/2);    %grid voltage B phase%
Vgc=Vg_rms*sin(wg*t- 4*pi/3 - pi/2);   %grid voltage C phase%
Vdc=400;
    Ts=0.02;
%     if (t<0.6)
%         Sref=200*ones(Hp,1);
%     end
%     if(t>=0.6&&t<=1.2)
%          Sref=250*ones(Hp,1);
%     end
%      if(t>1.2)
%          Sref=314*ones(Hp,1);
%     end
%     if (t<0.6)
%         Tl=85;
%     end
%     if(t>=0.6&&t<=1.2)
%          Tl=110;
%     end
%      if(t>1.2)
%          Tl=85;
%     end

    FF=phi'*(F*xf-Sref);
    gamma2=[(v_max-us)*ones(Hc,1);(-v_min+us)*ones(Hc,1)];
    gamma3 = [(y_max*ones(Hp,1))-F*xf;-y_min*ones(Hp,1)+F*xf];
    b=[gamma1;gamma2;gamma3];
    deltav=QPhild(E,FF,M,b);
    us=us+deltav(1);
    xm=Ad*xm+Bd*us;
   ym=Cd*xm;
```

```
    x(3)=ym;

     Iqref=us;
      e1=Idref-x(1);
      e2=Iqref-x(2);

      z1=z1+0.5*h*(ee1+e1);
      ee1=e1;
      z2=z2+0.5*h*(ee2+e2);
      u1=kp1*e1+ki1*z1;
      u2=kp2*e2+ki2*z2;
      ee2=e2;

      u=[u1;u2];
      x=RK4(@fun,t,x,u,h);
      ym=x(3);
      xf=[xm-xm_old;ym]; xm_old=xm;
      t=t+h;
      Te=120*(3*p*pm*Iqref)/2;
      w=30*x(3)/pi;
     ref=30*Sref(1)/pi;
     Vdg=u(1);
     Vqg=u(2);
     %Space vector PWM
     Vref=sqrt(Vdg.^2 + Vqg.^2);
phi_pwm = atan(Vqg/Vdg);
ang = mod(wg*t + (phi_pwm - pi/6)*ones(1,length(t)),(2*pi));
K=sqrt(3)*Ts*Vref./Vdc;

theta=ang;
alpha = mod((theta),(pi/3));
n=fix((theta)/(pi/3))+1;

T1=K.*(sin(n*(pi/3)- theta));
T2=K.*(sin(theta-(n-1)*(pi/3)));
To=(Ts-T1-T2)/2;

s1=(n==1).*(T1+T2+To)+(n==2).*(T1+T2+To)+(n==3).*(T1+To)+(n==4).*(To)+(n=
=5).*(To)+(n==6).*(T2+To);
s2=(n==1).*(To)+(n==2).*(T2+To)+(n==3).*(T1+T2+To)+(n==4).*(T1+T2+To)+(n=
=5).*(T1+To)+(n==6).*(To);
s3=(n==1).*(T1+To)+(n==2).*(To)+(n==3).*(To)+(n==4).*(T2+To)+(n==5).*(T1+
T2+To)+(n==6).*(T1+T2+To);

rs=rem(t,Ts);

sa=((s1)>rs);
sb=((s2)>rs);
sc=((s3)>rs);

Vsa=2*(sa-sb-sc).*Vdc/3;
Vsb=2*(sb-sa-sc).*Vdc/3;
Vsc=2*(sc-sa-sb).*Vdc/3;

% Vab = Vsa - Vsb;
% Vgab = Vga - Vgb;
     t=t+h;
     buf4=[buf4;t Vga Vgb Vgc];
     buf3=[buf3;t Vsa Vsb Vsc];
```

```
    buf2=[buf2;t s1 s2 s3];

    buf=[buf;t x(1) x(2) w us u' ref-w ref Te];
end
% plot(buf(:,3),buf(:,9))
% plot(t,Vsa);
% hold
% plot(buf4(:,1),buf4(:,2),buf4(:,1),buf4(:,3),buf4(:,1),buf4(:,4));
% ylabel('Vabc(V)','interpreter','Latex'),
xlabel('Time(Sec)','interpreter','Latex')
% figure;plot(t,Vsb,'y');
% hold;
% plot(t,Vgb,'r');
% figure;plot(t,Vsc,'g');
% hold;
% plot(t,Vgc,'r');
% figure(1)
% plot(buf2(:,1),buf2(:,2));
% hold;
% plot(buf2(:,1),buf2(:,3),'y');
% plot(buf2(:,1),buf2(:,4),'g');
% figure(2)
% plot(buf3(:,1),buf3(:,2));
% hold;
% plot(buf3(:,1),buf3(:,3),'y');
% plot(buf3(:,1),buf3(:,4),'g');
% stepinfo(buf(:,4),buf(:,1))
% figure(3)
% subplot 321
% plot(buf(:,1),buf(:,2),'linewidth',1.5)
% xlabel('t'), ylabel('id')
% subplot 323
% plot(buf(:,1),buf(:,3),'linewidth',1.5)
% xlabel('t'), ylabel('iq')
% subplot 325
stepinfo(buf(:,4),buf(:,1))
 figure(1)
%  subplot 321,
 plot(buf(:, 1), buf(:, 4),   'linewidth', 1.5), hold on
yline(ref,'k:','linewidth', 1.5)
%axis([0 2 -500 3500])
ylabel('Rotor Speed(RPM)','interprete','Latex'),
xlabel('Time(Sec)','interprete','Latex'),
legend('MPC','Ref','LQR','GA-PI')
hold on
figure(2)
plot(buf(:,1),buf(:,8),'linewidth',1.5)
ylabel('Error','interprete','Latex'),
xlabel('Time(sec)','interprete','Latex')
legend('MPC','LQR','GA-PI')
hold on
% % % %subplot 322, plot(buf(:, 1), buf(:, 7), 'linewidth', 1), hold on
% % subplot 323, stairs(buf(:, 1), buf(:, 2), 'linewidth', 1.5), hold on
% % legend('Id')
% % % %subplot 314, stairs(buf(:, 1), buf(:, 3), 'linewidth', 1), hold on
% % subplot 325, stairs(buf(:, 1), buf(:, 3), 'linewidth', 1.5), hold on
% % legend('Iq')
%  %subplot 322,
 figure(3)
 stairs(buf(:, 1), buf(:, 5), 'linewidth', 2), hold on
 yline(v_max,'k--','linewidth',1.5), yline(v_min,'k--','linewidth',1.5)
```

```
 ylabel('control signal(u)','interprete','Latex'),
xlabel('Time(Sec)','interprete','Latex'),legend('MPC','v\_max','v\_min','
LQR','GA-PI')

%  %axes('position', [0.25 0.175 0.25 0.25]);
% box on
% index=(t>0)&(t<0.4);
% plot(t(index),ym(index))
% axis tight
% figure(4)
% subplot 211, plot(buf(:,1),buf(:,2),'linewidth', 1.5),ylabel('Id
Current(A)','interprete','Latex'),xlabel('Time(Sec)','interprete','Latex'
)
% subplot 212, plot(buf(:,1),buf(:,3), 'linewidth', 1.5),ylabel('Iq
Current(A)','interprete','Latex'),xlabel('Time(Sec)','interprete','Latex'
)
% figure(5)
% subplot 211, plot(buf(:,1),buf(:,6),'linewidth', 1.5),ylabel('Control
Signal(Vd)','interprete','Latex'),xlabel('Time(Sec)','interprete','Latex'
), legend('Vd')
% subplot 212, plot(buf(:,1),buf(:,7), 'linewidth', 1.5),ylabel('Control
signal(Vq)','interprete','Latex'),xlabel('Time(Sec)','interprete','Latex'
) ,legend('Vq')
% % % %subplot 322, plot(buf(:, 1), buf(:, 7), 'linewidth', 1), hold on
% subplot 324, stairs(buf(:, 1), buf(:, 6), 'linewidth', 1.5), hold on
% legend('Vd')
% % %subplot 314, stairs(buf(:, 1), buf(:, 3), 'linewidth', 1), hold on
% subplot 326, stairs(buf(:, 1), buf(:, 7), 'linewidth', 1.5), hold on
% legend('Vq')
% figure(2)
% %electr
% figure(4)
% plot(buf(:,1),buf(:,10))

 %motor dynamics
function xdot=fun(t,x,u)
global R L pm p bbb  J Tl
R=0.05; L=6.35*10^-4;
pm=0.192; p=4; bbb=0.002; J=0.011;
a=R/L; bb=pm/L; c= (3*p)*pm/(2*J); d=bbb/J;
xdot=zeros(3,1);
xdot(1)=-a*x(1)+x(2)*x(3)+u(1)/L;
xdot(2)=-x(1)*x(3)-a*x(2)-bb*x(3)+u(2)/L;
xdot(3)=c*x(2)-d*x(3)-Tl*p/J;
end
```